博士論文(要約)

Synthesis of boron transport systems and analysis of boron toxicity mechanisms in roots of *Arabidopsis thaliana*

(シロイヌナズナの根におけるホウ素輸送の統合的理解と、過剰ホウ素による生育阻害機構の解明)

Naoyuki Sotta

反田 直之

Contents

Abbreviation

CDS, coding DNA sequence;

CEI cortex/endodermis initials;

CP, core particle;

cps, counts per second;

DAG, day after germination;

DAPI, 4',6-diamidino-2-phenylindole;

EdU, 5-ethynyl-2'-deoxyuridine;

EZ elongation zone;

ER , endoplasmic reticulum;

GFP, green fluorescent protein;

GUS, β-glucuronidase;

LA-ICP-MS, laser ablation-inductively coupled plasma-mass spectrometry;

MDA , mainly malondialdehyde;

MZ, meristem zone;

NBT, nitroblue tetrazolium;

PI, propidium iodide;

PM, plasma membrane;

PPB, pre-prophase band;

TBA , 2-thiobarbituric acid;

TPR, tetratricopeptide repeat;

QC, quiescent center;

ROI , region of interest;

RP, regulatory particle;

ROS, reactive oxygen species;

RT-PCR, reverse transcription-PCR;

SNP, single nucleotide polymorphism;

SSLP, single sequence length polymorphism

Ub, ubiquitin;

UPR, unfolded protein response;

QC , quiescent center;

Abstract

Boron is an essential element for plants. Boric acid is required for crosslinking of pectin side chains in cell walls, and boron deficiency hampers plant growth. Boron is toxic in excess for organisms including plants. Excess boron stress increase accumulation of DNA damage and causes developmental defects including cell death in root tips. Because of these properties, both deficiency and toxicity of boron have caused agricultural problem through the world. Approaches for this problem from plant biology can be at two different levels. One is at the level of transport, the other is at the usage or effect of boron in planta. It has been known that plants have developed boron transport system consists of multiple boron transporters with distinct functions for efficient boron uptake and maintenance of its homeostasis. Improvement of the transport system has been shown to provide plants tolerance to undesirable boron conditions. The other level, the effect of boron in planta, is to improve tolerance to deficient/excessive boron after uptake in planta. Understanding of molecular mechanisms of growth defects caused by inadequate boron dose would make it possible to propose strategy for breeding of tolerant plants.

This thesis is composed of five chapters and overall conclusions, with the central theme of “boron as a plant nutrient”. In Chapter 1, I established a 2-dimentional mathematical model to simulate boron transport through roots, which suggested distinct functions of root tips and other parts of roots in boron uptake. In Chapter 2, I demonstrated behavior of boron transport regulation system to propose significance of the swift regulation in preventing instability. In Chapter 3, I obtained experimiental evidences which suggest NADPH oxidase *RBOHC* is responsible for root growth inhibition under excess boron stress. In Chapter 4, I identified a transcription factor *NAC103* is involved in excess boron stress. Chapter5 is a subject developed from the course of this study. A previously uncharacterized gene *TPR5* was revealed to be crucial for root meristem maintenance and cell division.

Chapter1. Mathematical modelling and experimental validation of spatial distribution of boron in the root of *Arabidopsis thaliana* identify high boron accumulation in the tip and predict a distinct root tip uptake function

Boron is transported in roots of *Arabidopsis thaliana* mainly by two different types of transporters, BORs and NIPs. Both are plasma membrane-localized, but have distinct transport properties and patterns of cell-type specific accumulation with different polar localizations, which are likely to affect boron distribution. Here, I used mathematical modelling and an experimental determination to address boron distributions in the root. A computational model of the root is created at the cellular level, describing the boron transporters as observed experimentally. Boron is allowed to diffuse into roots, in cells and cell walls, and to be transported over plasma membranes, reflecting the properties of the different transporters. The model predicts that a region around the quiescent centre has a higher concentration of soluble boron than other portions. To experimentally evaluate this prediction, with collaborators, we determined boron distribution in roots using laser ablation-inductivity coupled plasma-mass spectrometry. The analysis indicated that boron concentration is highest near the tip and is lower in the more proximal region of the meristem zone, similar to the pattern of soluble boron distribution predicted by the model. The mathematical model also predicts that upward boron flux does not continuously increase from the root tip toward the mature region, indicating that boron taken up in the root tip is not efficiently transported to shoots. This suggests that root-tip absorbed boron is likely used for local root growth, and that instead it is the more mature root regions which bear a greater role in transporting boron toward the shoots.

Chapter2. Rapid transporter regulation prevents substrate flow traffic jams — a case study of boron transport

Nutrient uptake by roots often involves substrate-dependent regulated nutrient transporters. For robust uptake, the system requires a regulatory circuit within cells and a collective regulatory behaviour across the tissue. A paradigm for such systems is boron uptake, known for its directional transport and homeostasis, as boron is essential but also toxic at high concentrations. Boron uptake occurs via diffusion facilitators (NIPs) and exporters (BORs), each presenting distinct polarity. Intriguingly, although boron soil distributions are dynamically stable, both transporters manifest strikingly swift boron-dependent regulation. Through mathematical modelling, I demonstrated that slowing down regulation drives the root tissue to unstable and physiologically detrimental oscillatory behaviour. Cytosolic boron concentrations peaked to high, potentially cytotoxic, levels, whereas nutrient throughput to the xylem was hampered. I conclude that, while maintaining homeostasis, swift regulation of the transporters within a polarized tissue context is critical to prevent intrinsic traffic-jam like behaviour of nutrient flow.

Chapter3. NADPH oxidase *RBOHC* is responsible for root growth inhibition caused by excess B stress in *Arabidopsis thaliana*

Excess boron toxicity for plants has been a significant problem in agriculture and its prevention contributes better production. There have been a number of studies on boron toxicity, and several mechanisms are proposed, but the understanding of the molecular process of toxicity occurrence remains in many parts unclear. It has been reported that excess boron stress causes oxidative stress in

plants. In this chapter, I screened ROS production genes for excess boron stress inducibility in *A. thaliana* roots by microarray and studied their roles in root growth inhibition caused by excess boron stress. NADPH oxidase *RBOHC* is expressed mainly in the root elongation zone and induced by excess boron stress. A knockout mutant of *RBOHC* exhibited better root elongation under excess boron conditions while under the normal condition the growth difference was not evident. In the wild type, root meristem shrinks under high boron condition, but the extent of the meristem size reduction was significantly smaller in the *rbohc* mutant. These results suggest importance of *RBOHC* under high B condition. RBOHC is known to produce superoxide, an oxidation source, and I examined the extent of lipid peroxidation in roots, the tissue displays RBOHC dependent high boron response. Levels of lipid peroxidation under excess boron stress in roots were less in *rbohc* compared to that in the wild type, suggesting that *rbohc* mutant undergoes less oxidative stress under excess boron conditions. Taken together, I conclude that *RBOHC* is responsible for induction of oxidative stress and growth inhibition in roots under excess boron stress

Chapter4. A mutation in *ANAC103* alleviates DNA damage in *Arabidopsis thaliana* mutant sensitive to excess boron.

Excess boron (B) is toxic to plants, causing DNA damage accumulation and cell death in root meristems. However, the underling mechanisms which link boron and DNA damage remains unclear. It has been reported that *rpt5a-6*, a mutant of 26S proteasome, is sensitive to excess boron, exhibiting more frequent cell death in its root meristem and reduced root elongation. In this chapter, I revealed that reduction in root growth under high boron caused by the *rpt5a-6* mutation is suppressed by a mutation in a NAC domain containing transcription factor *NAC103*, a substrate of

proteasome, which functions in the unfolded protein response (UPR) pathway. The mutation in NAC103 alleviates excess-B-induced DNA damage accumulation and cell death in root meristems. Superoxide (O_2^-) staining with nitroblue tetrazolium (NBT) revealed that excess boron stress causes O_2^- accumulation in root tips and accumulation is higher in *rpt5a-6*, whereas the accumulation was reduced in *rpt5a-6 nac103-1* double mutant. Through the chapter, I demonstrate that regulation of *NAC103* through proteasome pathway is essential for root meristem maintenance under excess boron stress, and the involvement of *NAC103* in novel cellular processes.

Chapter5. TPR5 is involved in directional cell division and is essential for the maintenance of meristem cell organisation in *Arabidopsis thaliana*

Root growth in plants is achieved through the coordination of cell division and expansion. In higher plants, the radial structure of roots is formed during embryogenesis and maintained thereafter throughout development. Here I show that the tetratricopeptide repeat domain protein *TPR5* is necessary for maintaining radial structure and growth rates in *Arabidopsis thaliana* root. An *A. thaliana* mutant with reduced root growth was isolated and I determined that *TPR5* was the gene responsible for the phenotype. The *tpr5-1* mutant root growth rate was reduced to ~60% of that in wild-type plants. The radial structure was disturbed by the occurrence of occasional extra periclinal cell divisions. While the number of meristematic cells was reduced in the *tpr5* mutants, the cell length in the mature portion of the root did not differ from that of the wild type, suggesting that TPR5 is required for proper cell division but dispensable for cell elongation. Expression of the TPR5-GFP fusion protein driven by the *TPR5* promoter displayed fluorescence in the cytoplasm of root meristems, but not in mature root regions. DNA staining revealed that frequencies of

micronuclei were increased in root meristems of *tpr5* mutants. Through this study, I concluded that *TPR5* is involved in preventing formation of micronuclei, and is necessary for both the activity and directionality of cell division in root meristems.

In my Ph.D study, I revealed important aspects of boron transport and response to boron conditions in plants from two different approaches and their combinations. In the transport modeling, I established modering framework for boron transport and transporter regulations to capture the behavior of the system. In the experimental analysis of excess boron stress response, I revealed the involvement of two novel genes and illustrated a model for the mechanisms of growth inhibition caused by excess boron stress. Taken together I believe that my thesis represent a big heap in the understanding of boron as a plant nutrient.

Chapter1.

Mathematical modelling and experimental validation of spatial distribution of boron in the root of Arabidopsis thaliana identify high boron accumulation in the tip and predict a distinct root tip uptake function

Declaration

The research described in this chapter was conducted in collaboration with Dr. Akie Shimotohno, Mr. Takafumi Sato, Drs. Micol De Ruvo, Athanasius F.M. Marée, Verônica A. Grieneise, and Toru Fujiwara, and the portions of the studies conducted by the co-authors are indicated in the subtitles.

Abstract

Boron, an essential micronutrient, is transported in roots of *Arabidopsis thaliana* mainly by two different types of transporters, BORs and NIPs. Both are plasma membrane-localized, but have distinct transport properties and patterns of cell-type specific accumulation with different polar localizations, which are likely to affect boron distribution. Here, we used mathematical modelling and an experimental determination to address boron distributions in the root. A computational model of the root is created at the cellular level, describing the boron transporters as observed experimentally. Boron is allowed to diffuse into roots, in cells and cell walls, and to be transported over plasma membranes, reflecting the properties of the different transporters. The model predicts that a region around the quiescent centre has a higher concentration of soluble boron than other portions. To experimentally evaluate this prediction, we determined boron distribution in roots using laser ablation-inductivity coupled plasma-mass spectrometry. The analysis indicated that boron concentration is highest near the tip and is lower in the more proximal region of the meristem zone, similar to the pattern of soluble boron distribution predicted by the model. Our model also predicts

that upward boron flux does not continuously increase from the root tip toward the mature region, indicating that boron taken up in the root tip is not efficiently transported to shoots. This suggests that root-tip absorbed boron is likely used for local root growth, and that instead it is the more mature root regions which bear a greater role in transporting boron toward the shoots.

Introduction

Plant growth depends on nutrient uptake. Understanding the mechanisms and regulation of nutrient uptake is of fundamental biological importance. The process is crucial for crop production, so its understanding is also essential to achieve an efficient usage of nutrients in agriculture (Marschner, 1995, for review). A number of mineral nutrient transporters involved in nutrient uptake from the soil have been identified and characterized (Dean *et al.*, 2014, for review). In many cases, a particular mineral nutrient is transported by several transporters with different transport properties, while different nutrient transporters can exhibit distinct, cell-type specific accumulation (Slewinski 2011, for review). For a nutrient to be taken up by roots and transported to shoots, it needs to be taken up into symplasts and then loaded into the xylem, an apoplastic space. Uptake by root cells and loading into the xylem are thus controlled by influx and efflux transport, respectively, and in many cases both processes are facilitated by distinct transporters with different properties.

Boron is an essential micronutrient for plants, but toxic in excess (Warington, 1923, Miwa and Fujiwara, 2010 for review). Its deficiency causes severe defects in vegetative and reproductive growth (Shorrocks, 1997 for review), but excess boron also causes growth defects (Nable *et al.*, 1997, Shorrocks, 1997 for review). Hence it is important for plant growth to maintain boron homeostasis. To achieve homeostasis, the spatial organization of transport processes plays a crucial role.

Boron is taken up from the soil by plant roots through an elaborate spatial network of transport proteins, which are differently expressed in each cell type and, moreover, can be localized in a highly polar fashion along the cells' plasma membrane (PM). In *Arabidopsis thaliana* we have identified several transporters of boron that are required for efficient uptake by roots, transport to shoots, preferential distribution in shoots and excluding excess boron from roots (Takano *et al.*, 2001, Takano *et al.*, 2002, Takano *et al.*, 2006, Miwa *et al.*, 2007, Miwa *et al.*, 2011, Miwa *et al.*, 2013). Two main classes of boron transporters account for the facilitated transport of boron, in the form of boric acid, through the plant tissue: Noduline26-like intrinsic proteins (NIPs) allow for an increased unbiased bidirectional movement of boric acid across the PM, while BOR1/BOR2 account for a facilitated efflux of boric acid out of the cell into the cell wall. Specifically, NIP5;1 is required for efficient uptake of boron from soil to the root (Takano *et al.*, 2006). BOR1 is an efflux transporter of boron and required for efficient transport of boron from roots to shoots. BOR2, the closest homologue of BOR1, is important for root growth under low boron condition and enhances crosslinking of pectic polysaccharides in the cell wall (Miwa *et al.*, 2013). In aerial portion of plants, BOR1 and NIP6;1, the closest homologue of NIP5;1, play an important role for efficient preferential transport of boron to young portions of shoots (Takano *et al.*, 2001, Tanaka *et al.*, 2008).

Among the transporters identified, BOR1, BOR2, and NIP5;1 are important for boron transport in roots. These transporters have distinct cell-type specificity of expression and polar localization pattern (Takano *et al.*, 2010, Miwa *et al.*, 2013). In general, BOR1 and BOR2 exhibit "inner" localization while NIP5;1 exhibits "outer" localization. We expect that the presence of different transporters with different properties in terms of cell specificity and polarity should give rise to a characteristic pattern of boron distribution in the root, and that such a pattern could affect the overall flux of boron through the root. As boron passes through the plant tissue, it can get cross-linked and incorporated into the cell wall, which is essential for establishing correct cell wall

properties and hence plant growth. Xylem loading is likewise essential, to deliver boron to the growing shoot and leaves. Nevertheless, in the root tip – in the absence of mature vascular systems – a striking level of complexity can be observed in the spatial patterning of the transporters, both on the cellular and on the tissue scale. It is as yet unclear what functionality or behaviour this patterning manifests.

Despite the great advances in molecular and genetic studies on boron uptake in plants, until now we could only indirectly estimate how the removal or change of certain transporters would impact boron movements and concentrations within the root. Boron measurements have only been performed at the tissue or plant level or through xylem loading assays in plant levels (Takano et al., 2002). Such coarse-grained data was valuable to estimate approximate behaviours of mutants, but cannot reveal boron distributions within tissues.

In this study, to elucidate the boron distribution pattern in the root tip, we adopted two different approaches, namely mathematical modelling and an experimental demonstration of the boron distribution in the root. For the mathematical modelling, we developed a description of the diffusion and BOR1/BOR2- and NIP5;1-facilitated boron transport in and across cells and cell walls in a structured root layout. A similar approach has been successfully adopted for the modelling of auxin transport (Grieneisen *et al.*, 2007).

For the experimental approach, we utilized laser ablation inductivity coupled plasma-mass spectrometry (LA-ICP-MS). This method was originally developed for the determination of elements in solid samples at micrometer-scale resolution (Audétat *et al.*, 1998, Chi *et al.*, 2002). LA-ICP-MS also allows us to obtain elemental distributions in biological samples (Wang *et al*., 1994, Punshon *et al*., 2004). Although the technique has a strength in being able to obtain high spatial resolution of the elemental distributions, the major drawback for the analysis of biological materials is the need of pretreatments or fixation, which could affect the distribution of elements (Koelmel *et*

al., 2013, da Silva and Arruda, 2013, Lefèvre *et al.*, 2014). In the present study, we therefore developed a method to determine boron distribution in the root of *A. thaliana* without the need of fixation, by reducing the duration of the experiment.

Comparison of the simulation outputs and experimental data of the boron distribution in roots allowed us to propose that *A. thaliana* roots have two functional domains with different physiological roles in terms of boron transport and boron utilization.

Results and Discussion

Establishment of a spatial model to describe boron distribution in A. thaliana roots

Declaration: The basic code framework for the simulation was provided by Drs. Athanasius F.M. Marée, Verônica A. Grieneise. The root layout of the model was improved by Drs. Micol De Ruvo and Takafumi Sato.

We constructed a two-dimensional model for boron transport within the spatial setting of the *A. thaliana* root, to assess what patterning would be expected in the Arabidopsis root when the combined action is taken into account of known (i) levels and localization of boron efflux facilitators (BOR1 and BOR2), (ii) levels and localization of NIP5;1, which enhances the diffusive (i.e. bidirectional) permeability of boron, and (iii) intracellular and extracellular diffusion of soluble boron. Many of the previous nutrient transport models describe cells as units containing only a single concentration value. Given the polar localization of the transporters, it is possible that boron concentrations within a cell or the cell wall could manifest spatial patterning. Hence, to be able to simulate such features, we took subcellular spatial structures explicitly into account. Given that only the soluble form of boron diffuses, is able to cross membranes and interacts with the transporters, we

only consider this form within the model, ignoring all transitions between the soluble and solid form. Our computational framework thus describes boron diffusion within cells and within the cell wall, as well as BOR and NIP-mediated boron transport across membranes. It does so by numerically solving partial differential equations with complex boundary conditions using alternating-implicit direction methods, which has previously been extensively used to perform simulations on auxin dynamics (Grieneisen *et al.*, 2007, Grieneisen *et al.*, 2012). For further details on the equations and numerical simulations, see Materials and Methods. More recently, modifications to the spatial layout of the root tip have been incorporated and used to take into account the more refined detail of the cell types of the root tip and stem cell niche, their shape and polarity (see also Cruz-Ramírez *et al.*, 2012). We based, and further developed, the spatial layout of our current work on this advanced and validated layout. Our current spatial setting thus captures all cell types in the stem cell niche as well as overall differences in cell lengths at more proximal regions of the root (Figure 1-1A). The root is therefore longitudionally divided into a Meristem Zone (MZ), an Elongation Zone (EZ) and a Differentiation Zone (DZ), as reported in Laskowski *et al.*, 2008, with moreover variable cell lengths within the EZ. Critical to the outcome of the model is the positioning of the transporters, which, together with the spatial root context, result in the complex flux patterns underlying the concentration profiles. Through careful analysis of BOR1 and BOR2-GFP lines, and in accordance to previously published expression and localization patterns, we positioned these efflux facilitators on the cell membranes in a similar and characteristic manner, in which the simulated BORs represent all BORs in the root, and the simulated NIPs represent all the NIPs in the root (Figure 1-1B, Takano *et al.*, 2010, Miwa *et al.*, 2013). BORs are mostly represented by BOR1 and BOR2, as these are the only two BOR transporters whose disruption causes severe growth defect under low boron conditions among the seven members of BORs in *A. thaliana* (Takano *et al.*, 2002, Miwa *et al.*, 2013). NIPs are mostly represented by NIP5;1 as it is the only gene whose disruption causes severe growth defect under low

boron conditions among *A. thaliana* NIPs (Takano *et al.*, 2006). To allow for polarized transporter localization, we divided the PM of each cell into eight distinct zones, depending on its orientation directing inwards or outwards, and upwards (shootwards) or downwards (rootwards) (Figure 1-1C). This enabled us to critically analyse experimental images and incorporate *in silico* which of those eight zones, for each individual cell type, presented transporter localization. Note that the density of BOR proteins differs both between cell types and along the longitudinal axis of the root. We captured this in the model by assuming three distinct levels of efflux permeability strengths due to BOR action: high, medium and low. Similarly, we analysed the NIP5;1 levels and localization patterns, and modelled what we considered the representative positions of these proteins, again, subdividing their levels (and hence permeability strengths) into three categories. Regarding NIP5;1, some experimental images suggest that they might reside at low levels in the vascular tissue, although the experimental evidence is not conclusive. We have therefore considered both possibilities, as will be discussed below.

BORs were set to allow for unidirectional efflux transport of boron and its transport is dependent on the local concentration of boron within the cell at the PM, while NIPs were set to allow for bidirectional boron transport over the PM. Also a background boron permeability over the PM allows bidirectional diffusion of boron (Figure 1-1D). Given the absence of any quantitative data from which saturation in boron transport could be derived, we here considered a purely linear relationship between observed transporter density and enhanced permeability, as well as between the soluble boron concentration and the flux over the PM. Note that as a consequence of such an assumption, different boron levels in the medium result in the same relative pattern in boron concentration in the model, scaled by the medium concentration used (as long as no changes in transporter levels or localization are explicitly introduced).

The simulations consider a fixed boron concentration in the medium, which then can

diffuse into the cell wall that surrounds the root with a rate equal to the diffusion rate within the cell wall. In this study we focus on the very tip of the root, hence we do not simulate the xylem and its convective flow shootwards. The proximal boundary condition, however, is such that we allow soluble boron to flow out of the vasculature at the very end of the *in silico* root, as if it were connected to further vascular cells (see Cruz-Ramírez *et al.*, 2012 for a detailed description of how this is implemented). In each simulation, we consider the initial concentrations within the whole root tissue to be zero, and as boron from the medium starts to diffuse in, a pattern in boron distribution emerges. The profiles shown were obtained after allowing the simulation to achieve a steady state distribution.

Predicted spatial distribution of soluble boron in the root.

With the given settings, we simulated boron transport from the soil into the root. The concentration of boron in the medium was set to 0.3 µM, the initial concentration of boron in the root was set to 0 µM, and transport dynamics were simulated until a steady state was reached (Figure 1-2A). The resulting boron concentration profile exhibited a pattern in which the concentration near the root tip was higher than in the other portions of the root. Boron concentration in the cell wall was always much higher than that in the cells (Figure 1-2B,C), which can be easily understood as BORs drive the efflux of boron into cell wall, while NIPs affect import and export in an equal fashion. Cell wall concentration is therefore inevitably always higher than the cytosolic concentration. Combined with the polarized NIP localization, the high concentration of boron in the cell wall drives a large directed flux of boron into the inner neighbouring cells. It accumulates in the quiescent centre (QC), while also the concentration of boron in the vascular tissue is slightly higher than in the surrounding cell types. The overall concentration of boron becomes low in the upper portion of roots (see further discussion below). Such a pattern becomes apparent after 200 min from the initiation of the

simulation, and does not change dramatically during the next 600 min (Figure 1-2).

Boron determination of gel samples with LA-ICP-MS

Declaration: Operation of LA-ICP-MS was performed by Dr. Akie Shimotohno.

To experimentally determine the actual boron distribution in the roots of *A. thaliana*, we set up an LA-ICP-MS system as shown in Figure 1-3. Plant materials were placed in the chamber in which a laser beam with a focal diameter of 10 μm is applied to the samples, and the ablated materials were then carried into ICP-MS by He gas (600 ml min^{-1}). The volume of the chamber and the passage to ICP-MS is about 300 ml and the ablated materials are detected with about 20 second delay from the moment of ablation. We continuously recorded an arbitrary value, in count per second (cps), representing ^{11}B. From those values an arbitrary boron count for a laser beam shot could be calculated, by integrating the peak representing the ablation. The parameter setting of the LA-ICP-MS is described in Table 1-2.

Before analysing plant samples, we first established the relationship between the count obtained through LA-ICP-MS analysis and the boron content in the samples. Boric acid under a series of solution concentrations was solidified with gellan gum (1.5 % (w/v)) to form a sheet of gel with a 0.5 mm in thickness. Pieces of the gel sheet were subjected to LA-ICP-MS analysis. In one set of irradiation experiments, one spot on the sheet was irradiated by laser pulses of 4-6 nano-sec for 25 times within 5 seconds, followed by the irradiation of a next spot. Each spot then repeatedly received additional irradiation bombardments, until the signal produced by the irradiation became less than three times of the background fluctuation. At that moment we assumed that the complete 0.5 mm deep column had been ablated. We then calculated the total count for each spot as the sum of the counts of all detectable shots at that spot. As indicated in Figure 1-4A, the

accumulative count from the LA-ICP-MS of such a set of shots at a single spot increases almost linearly in proportion to the concentration of boron in the gel. The conversion ratio of signal count to boric acid concentration in the gel is 953 count/μM boric acid (Figure 1-4A). In this experiment, the volume of the gels that were ablated is that of a cylinder of 10 μm in diameter having a depth of 500 μm. Given this volume, we estimate the ratio between the count obtained by LA-ICP-MS and the amount of ablated boron in the gel to be 4×10^{-5} fmol/count.

Determination of boron in *A. thaliana* root using LA-ICP-MS

Declaration: Operation of LA-ICP-MS and determination of the ratio of soluble boron to the total boron was performed by Dr. Akie Shimotohno.

We then examined *A. thaliana* seedlings. Col-0 were grown for five days after germination on MGRL media (Fujiwara *et al.*, 1992), solidified with 1 % (w/v) gellan gum containing 0.3 μM boric acid and subjected to the analysis. The very tip of the root was identified with the microscope attached to the LA equipment, and from the tip 11 spots with 10 μm in diameter each were laser ablated, with 30 μm intervals between the centres of the spots. Ablation of the 11 spots was carried out in sequence, and the same sequence was repeated several times, until the signal intensity became less than three times the background fluctuation. Typically the forth sequence gave a signal indistinguishable from the background level. The laser ablations were repeatedly done at precisely the same spots, we assured ourselves that after several shots the spots of the laser ablation were almost perfect circles of 10 μm in diameter (Figure 1-3B). We therefore conclude that in most cases three shots at the same spot are sufficient to completely penetrate transversally through the root tissue.

The average counts for each spot from wild type roots ranged between 1,500, in the

proximal region of the roots where the signal was low, and 10,000, in the QC area (Figure 1-4B). Using the conversion ratio of 4×10^{-5} fmol/count derived above, this is equivalent to 0.06-0.4 fmol and it is reasonable to assume that this amount of boron is derived from a cylinder of root tissue of 10 µm in diameter and the typical root thickness of 175 µm in length, which would make 0.06-0.4 fmol correspond to 4-30 pmol mm^{-3}. Miwa *et al*. (2013) determined total boron concentration in wild type roots grown with 0.1 µM boric acid to be 0.39 mmol/kg dry weight. Assuming that the dry weight of the root is 15% of the fresh weight, the total amount of boron in a cylinder of root tissue with 10 µm in diameter and 175 µm in length would be 0.8 fmol if boron were distributed homogeneously in roots, or 59 pmol mm^{-3}. This is, depending on the location along the root, about 2-15 times higher than the amounts obtained from the LA-ICP-MS analysis, and on average 10 times higher. In the study by Miwa *et al*. (2013), the total concentration of boron in the whole root was determined for plants grown with 0.1 µM boric acid for 10-14 days. We should therefore take into consideration that at that stage of the growth it is likely that the majority of the root samples analysed would be derived from the mature portion of the roots, for which we do not have LA-ICP-MS measurements. Another factor to take into account is that in the present analysis we used seedlings grown with 0.3 µM boric acid, so the total boron concentration in our samples is likely higher than what is to be expected with 0.1 µM boric acid.

Nevertheless, we conclude that the fraction of boron determined by LA-ICP-MS seems to represent only about, or less than, 10% of total boron in the cylinder. Under low boron supply, it is known that most of the boron in plants is present in the cell wall bound form (Matoh *et al.*, 1992). It is possible that LA-ICP-MS determines free soluble boron much more efficiently than the cell-wall bound boron, and that this is the underlying cause of the discrepancy. To further support our assumption, we determined the ratio of soluble boron to the total boron in roots grown with 0.3 µM boric acid, as described in the Materials and Methods. It was found that 14±4% (mean ± SD, n=3)

of boron was in soluble fraction, which is a reasonable agreement with our above mentioned assumption.

To further analyse if this could make sense, we compared the experimental results with the mathematical simulation. We did this by calculating from the model the amount of boron that would be measured with the LA-ICP-MS method if the technique were to be applied to our *in silico* root. Given that in our LA-ICP-MS analysis we ablated root samples in the shape of cylinder with a diameter of 10 µm and a depth of 175 µm, and the boron in this cylinder was taken into the ICP-MS for determination, we therefore calculated the predicted amount of boron that would be contained in a virtual cylinder, integrating boron concentrations over a 10 µm diameter and with a 175 µm depth, its hypothetical centre positioned at any possible location along the *in silico* root (Figure 1-4C). In support of the notion that the LA-ICP-MS analysis measures soluble boron, our modelling, which does not take bound boron into account, predicts very comparable boron amounts as measured in the experiments when using the final, equilibrium concentrations from the simulation. Furthermore, the model also predicted that in the absence of NIPs in the *in silico* root, the predicted boron concentrations would become very low (Figure 1-4C). We therefore used our LA-ICP-MS analysis to look at the *nip5;1* mutant, again grown with 0.3 µM boric acid. It did not provide us with any detectable signal, even though the same positions from the root tips were ablated as in the experiment with wild type, suggesting that the amount of boron detectable with LA-ICP-MS is greatly reduced in the *nip5;1* mutant, closely corresponding to the modelling prediction. In contrast, it has been determined by Takano *et al.,* (2006) that the total boron in the *nip5;1* mutant grown with 3 µM boric acid is reduced to 60% of the wild type, suggesting that reduction of the total amount of boron in the *nip5;1* mutant is not so dramatic. Combining our observation with the fact that the boron that we simulate in our mathematical model is soluble boron only and the fact that in our LA-ICP-MS analysis the *nip5;1* mutant did not give any detectable signal implies that boron

determined through LA-ICP-MS probably represents soluble boron.

Based upon the above-mentioned observations and considerations, we therefore assumed that the boron determined by LA-ICP-MS predominantly represents the soluble fraction of boron in roots. We do not know at this moment why LA-ICP-MS specifically detects soluble boron rather than also measuring cell-wall bound boron. It may be that soluble boron is more readily ablated and efficiently taken into ICP-MS, whereas the cell-wall bound boron is more resistant to ablation, or the ablated cell wall material may be less able to reach ICP-MS for detection.

Determination of spatial distribution of boron along the distance from the root tip in *A. thaliana* roots

Declaration: Operation of LA-ICP-MS was performed by Dr. Akie Shimotohno.

Experimental measurements on the wild type gave a boron distribution pattern along the distance from the root tip as shown in Figure 1-4B. Boron was high in the first two shot positions and then gradually declined as the shots moved further away from the tip. We compared this distribution with the one predicted by the mathematical simulation, shown in Figure 1-4C. The distribution obtained from the simulation is similar to the experimental data, with high boron levels at the root tip and a gradual decrease when moving away from the tip, as well as an equivalent concentration range, as discussed above. We acknowledge that the peak position and peak pattern are not identical between simulation and the experimental data. This could be due to the difficulty in locating the tip of the roots in the LA-ICP-MS experiments or to detailed differences in the distribution of transporters in the in silico root. Overall, we concluded that the experimentally found boron distribution pattern is reasonably similar to the pattern predicted by the model. This suggests that our model is capturing the major features of boron transport and distribution in the root.

We also conclude from our LA-ICP-MS analysis and mathematical modelling that boron concentration is high in the tip region of *A. thaliana* roots. Although we do not know what biological advantage high boron in the root tip region of roots yields, we would like to speculate on possible roles of this distribution. It was demonstrated 40 years ago that root elongation stops very quickly (within 30 min) after removal of boron from the medium (Kouch and Kumazawa, 1975). Hence it is possible that a high boron concentration is required in the tip to maintain its growth. If indeed a high concentration of boron in the root tip is required for growth, this would create a risky situation, since a high concentration of boron is toxic to living organisms, irrespective of the kingdom. In fact, even relatively small fluctuations in the boron conditions could further augment high boron toxicity problems. In agreement with these findings, it has been established that high-boron-induced DNA damage and related cell death is predominantly observed in the tip regions (Sakamoto *et al.*, 2011). It is possible that relatively strict regulation of boron homeostasis is needed to maintain high boron levels in the root tip while avoiding boron toxicity problems.

Consideration of the possible contribution of NIPs in the vascular tissues

Our model also predicted very high boron concentrations in the vascular cell walls, presenting large differences between high apoplastic values versus low cytoplasmic concentrations (Figure 1-2B,C). This was due to the fact that in our model vascular cells were endowed with BOR proteins, but did not possess NIP transporters to enhance the uptake in the next cell shootwards. To analyse its implications, we studied the predicted resulting shootwards fluxes within the root. Our mathematical model straightforwardly allows us to calculate the upward flux of boron along the distance from the root tip.

Surprisingly, we found that the net shootwards fluxes were extremely low (Figure 1-5A).

The flux is reasonably high up to 500 µm from the tip, but it becomes very low in the region further away from the tip. This means that in this model, boron taken up by the tip of the roots is not efficiently transported shootwards, and a substantial portion of boron "leaks" out back into soil from the cell wall in the more proximal region of the MZ. We considered that this scenario is conceptually strange, given that boron uptake requires energy and boron taken up by NIPs and BORs in the tip region in expense of energy should hence be efficiently transported to shoots, by means of loading the xylem for further shootwards transport (which only initiates around 2mm from the tip, which is why it is not included in this model). In contrast, the model predicted that unused boron (i.e. the soluble boron that does get built into the cell wall in the MZ/EZ) would effectively get lost while being transported upwards (i.e. leave the root again), before it is able to reach the region where functional xylem starts.

Given that this loss of boron is a direct consequence of the high boron levels in the vasculature and the outwards flux through the apoplast it triggers, we hypothesised that weak vascular NIP5;1 signalling that could be observed in some images of NIP5;1-GFP lines might represent actual and functional vascular transporters. When we implemented this into the model, by positioning weak NIP transporter expression within the vascular tissue (Figure 1-5B), we found that, in contrast to the previous results, simulations now predicted a high net shootwards flux (Figure 1-5C). Even low densities of NIP transporters were sufficient to cause a strong positive effect on shootwards boron throughput. The reason for this is that now, instead of the root effectively loosing boron at each cell wall interface, diffusing apoplastically outwards back into the medium, the neighbouring vascular cells are capable of taking up the soluble boron again, followed by directional transport due to polarly localized BOR1, bringing it into the cell wall to be taken up again by the next cell and so forth – all the way up until it reaches the point at which a functional xylem has been established.

Although the flux pattern predicted by our alternative hypothesis (Figure 1-5C) indicated that the

meristem and its intricate spatial network of transporters could function as an entry point of boron into the plant, the resulting concentration pattern turned out not to be in accordance with the experimentally measured values (Figure 1-5D). Although it still correctly presented the characteristic high peak of soluble boron at the QC area of the root (alike the LA-ICP-MS measurements), it now failed to show the subsequent decreasing pattern in soluble boron content. Instead, when following the boron concentration in the shootwards direction, after a small decrease a subsequent strong increase in boron is predicted within the experimentally measured root area. We explored possible ways of "correcting" this profile by means of various assumptions regarding NIP localization in the cortex and endodermis (data not shown), but found that this general feature of the profile was robust, due to the close link between boron containment and an increasing profile: Boron enters everywhere along the root, and then gets transported upwards. If boron is not lost again during this process, more proximal cross-sections through the root must inevitably present larger boron fluxes. Increasing fluxes can only be accompanied by decreasing concentrations if there were a very steep shootwards gradient in transport efficiency, requiring an accompanying steep gradient in transporter levels. The latter, however, is not observed experimentally. We therefore conclude that – contrary to what might previously have been expected – the root tip does not function as an entry gate to bring boron to the shoot.

Given that the LA-ICP-MS results are consistent with lack of NIP in the vasculature, this led us to conclude that boron transport in the root tip area does not give rise to a functional net flux shootwards, motivating us to reconsider the functional role of the root meristem tips regarding boron. Together with the prediction that root tip dynamics generate extremely high vascular cell wall concentrations, our combined experimental and theoretical results suggests that soluble boron in the cell wall of the root tip is seemingly more important than previously considered, possibly because of the high rate of new cell wall formation as a consequence of the high division rates in the MZ. This

opens further cell biological and cell wall related questions for future investigation.

These findings suggest a functional division in the root. The tip region takes up boron and accumulates it at the “tip”, but this boron does not contribute strongly to the transport to shoots. Boron requirement is known to be high in the growing portion of plants and it is reasonable for the root growth to maintain the boron in the tip for the proper growth.

Conclusion

Our mathematical modelling and experimental determination of the boron distribution in *A. thaliana* roots demonstrated an accumulation of high boron in the tip of roots. We also concluded that two different functional domains are likely to be present in the roots in terms of boron uptake. In the tip, boron is taken up and used for the growth, while boron transported to the aerial portion is taken up from more mature portions of the roots.

Materials and Methods

Simulation for boron transport in root

Simulations of boron transport in *Arabidopsis thaliana* root were conducted using a grid-based two-dimensional spatial model. Our model consists of 2751 x 355 square grid points, each representing 0.5 × 0.5 μm, giving rise to a root 175 μm in diameter, corresponding to our observations of typical roots. The framework of the model followed Grieneisen *et al*. (2007), in which the spatial auxin distribution in the root was analysed by means of simulating diffusion and transport by auxin transporters. Each grid point is allocated to be part of cytosol, cell wall or media; interfaces between cytosol and cell wall represent membranes, and interfaces between media and the root represent the root-soil interface. BORs and NIPs, which are the boron efflux transporters and permeability facilitators respectively, were located along the cytosolic boundaries according to

observed localization patterns of recombinant proteins (Takano *et al.*, 2010, Kasai *et al.*, 2011, Miwa *et al.*, 2013). The layout of the root was improved from both the original and a more recent model (Grieneisen *et al.*, 2007, Cruz-Ramírez *et al.*, 2012), based on detailed experimental observations of *A. thaliana* roots (Figure 1-1A). Boron diffusion and transport was calculated numerically on the discretised grid points. Diffusion and permeability were dealt with independently. Diffusion only takes place within cells or within the cell wall, and its rate depends on whether the grid points represent cell or cell wall. Permeability is involved whenever two grid points are separated by a PM. The permeability rates, which can be different for boron entering the cell compared to leaving the cell, depend on the type and density of the transporters that are located at that specific piece of PM (Figure 1-1C). Reasonable parameter values are being used for both diffusion and permeability (Table 1-1).

Specifically, soluble boron is allowed to diffuse freely within cells, as well as within the apoplast, at a lower rate. Diffusion occurs in accordance with Fick's law:

$$\vec{J} = -D\vec{\nabla}B$$

where $\vec{J}$ represents the flux of boron within a contiguous space, D is the diffusion coefficient, and and $\vec{\nabla}B$ represents the local gradient in soluble Boron levels. The diffusion rate of boron in the cytoplasm was assumed to be 1100 $\mu m^2\ s^{-1}$, based on the boron diffusion rate in water (Goli *et al.*, 2010). The diffusion in the cell wall was assumed to be 15 times slower than in the cytoplasm, based on measurements of carboxyfluorescein diffusion (Kramer *et al.*, 2007), which is expected to have a negative charge in the cell wall, as is the case for boric acid.

However, whilst soluble boron can diffuse freely within cells and apoplastic spaces, the cell membrane represents a barrier to boron diffusive flux. PM is represented in our model by the interfaces between grid points representing the cellular compartments and the apoplastic cell wall. We consider a small level of “leakage” across the membrane, which is incorporated as a background

permeability term, p_m), without directional preference. When NIP is localized at a membrane interface, this enhances the bidirectional passage (p_{NIP}), while the BOR-family transporters facilitate only the efflux of soluble boron out of the cell (p_{BOR}). Thus, the flux of soluble boron across the cell membrane is described in our simulations by the following equation:

$$\vec{J} = -(p_{BOR}\hat{n})B_{in} + (p_{NIP}\hat{n})B_{out} - (p_{NIP}\hat{n})B_{in} + (p_m\hat{n})B_{out} - (p_m\hat{n})B_{in}$$

where $\hat{n}$ is the inward directed unit vector perpendicular to the membrane, B_{in} and B_{out} represent the soluble boron concentrations immediately adjacent to the membrane, at the cytosolic and cell wall side respectively, p_{NIP} represents the permeability rate due to NIP, and p_{BOR} represents the efflux permeability rate due to BOR. Note that if transporters are present (so that p_{NIP} and p_{BOR} take up non-zero values), three possible levels for the permeability due to BORs and NIPs can be assigned, high, medium or low, reflecting observed differences among tissue types in localisation intensity of recombinant protein (Figure 1-1B).

Laser ablation inductively coupled plasma-mass spectrometry (LA-ICP-MS) analysis

Boron concentration was measured using the inductively coupled plasma-mass spectrometry (ICP-MS, model SPQ9700; Seiko instrument Industry, Japan), interfaced with a laser ablation system (New Wave Research UP 213, Fremont, CA, USA). Laser ablation was performed in line scanning mode, the other ablation parameters are summarized in Table 1-2. Spots on the roots were observed with confocal microscope optics (FV1000; Olympus). The ICP-MS was set up in time-resolved analysis mode and the resultant boron amounts were reported in counts per second (cps). The data was plotted and the total count of the boron signal was calculated using ImageJ 1.46r by manual identification of the shapes of the peaks. A peak was defined as having a more than threefold larger area than the background. Baselines were determined as the averages of the highest and lowest background cps values during the five seconds before and after the peak. Signals with

an area less than three times the background were considered to be background themselves and treated as non-detectable.

Sample preparation for LA-ICP-MS

Wild type (Col-0) *A. thaliana* seeds were sterilized with 10 % (v/v) bleach and 0.1 % (v/v) Co-op K soft dish detergent (CO-OP Co., Ltd., Japan), and grown on the MGRL plate containing 2 % (w/v) sucrose and 0.3 μM boric acid, and 1.5 % (w/v) gellan gum (Wako Pure Chemical, Inc., Osaka, Japan), under controlled environmental condition (at 22^{o}C under a 16-h light/8-h dark cycle), as described previously (Fujiwara *et al.*, 1992; Takano *et al.*, 2006; Miwa *et al.*, 2013). The whole seedlings at five days after germination were placed on the glass slides attached by double-sided adhesive tape (Nichiban Co., Ltd., Japan), and used for laser ablation-inductively coupled plasma-mass spectrometry (LA-ICP-MS) analysis. Ablating the double-sided adhesive tape confirmed that the tape did not contain detectable boron. Since no suitable matrix-matched internal controls for *A. thaliana* seedlings was available, we alternatively prepared 1.5 % (w/v) gellan gum MGRL plates containing different concentration of boric acid (0, 0.3, 3, 5, 10 and 30 μM) for calibration standards. The resultant pieces of solidified gellan gum or *A. thaliana* whole seedlings were immediately placed on the glass slides and used for further LA-ICP-MS analysis.

Determination of soluble boron fraction

A. thaliana 5DAG wild-type seedlings grown on MGRL medium containing 0.3 μM boric acid were used for compartmental analysis. The sample preparation was conducted according to Dannel *et al*., (1998) with modifications. About 100mg of fresh root materials were frozen and thawed to burst cell wall, and centrifuged at 14k rpm for 10 min. Supernatant was taken as soluble fraction and resultant cell pellet were rinsed with double distilled water for four times. Rinsed material containing cell wall

bound boron and the resultant soluble fractions were digested with nitric acid and applied for further ICP-MS analysis. The ratio of boron in soluble fraction was calculated as the amounts of boron in the soluble fraction/combined amounts of boron in the soluble fraction and the pellet.

Acknowledgements

We would like to thank Y. Kawara for excellent technical assistance and T. Hakoyama for help with LA-ICP-MS. This work was supported in part by grants from the JSPS (Grant-in-Aid for Scientific Research number 21228002) to T.F. V.A.G. and A.F.M.M. were supported by the UK Biological and Biotechnology Research Council (BBSRC) via grant BB/J004553/1 to the John Innes Centre.

Figures

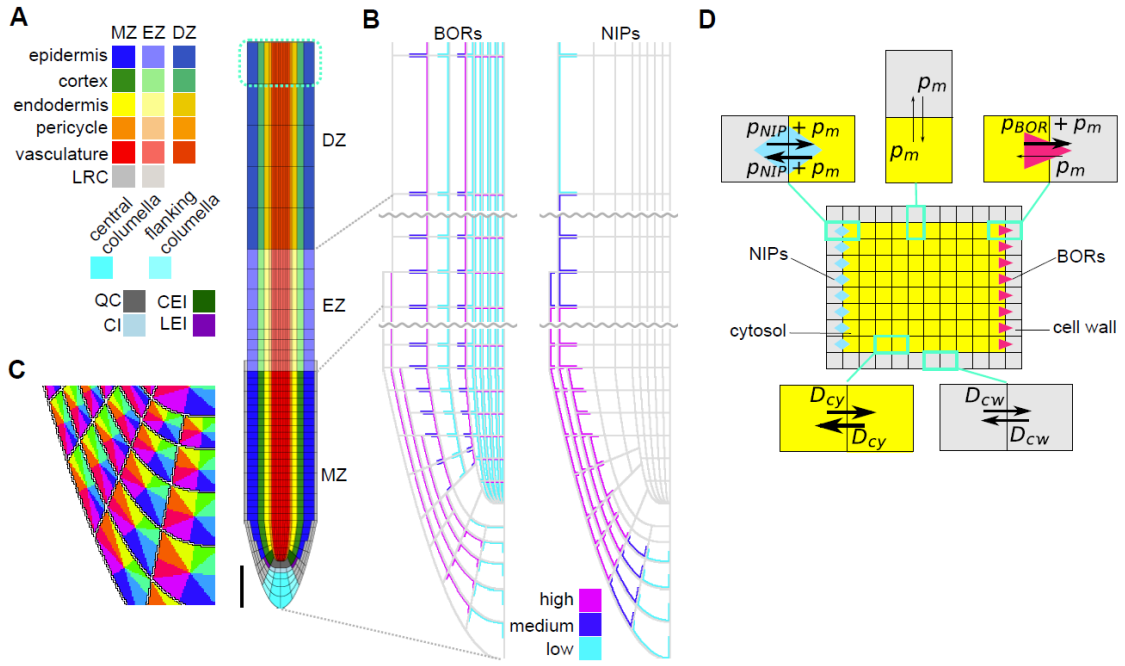

Figure 1-1 Spatial diffusion model for boron transport simulation.

(A) Root layout of the spatial model. The root consists of cell wall and cells, which are classified into 23 cell types. To describe the boundary condition at the proximal end of the plant, boron concentrations in the top cells that are surrounded by cyan dashed lines were fixed to zero, effectively capturing a shootwards boron flux. MZ, meristem zone; EZ, elongation zone; DZ, differentiation zone, LRC, lateral root cap; QC, quiescent centre; CEI, cortex/endodermis initial; CI, columella initial; LEI, lateral root cap/epidermis initial. Scale bar, 100 µm.

(B) Layout of BORs and NIPs in the root. BORs and NIPs were localized in the boundary between cell walls (grey) and cells. BORs and NIPS were assigned three different intensities, based upon experimental observations. Each cell type has an identical transporter localization.

(C) Each cell surface was divided into eight regions to allow for a detailed matching between experimental observations and the model regarding transporter localization.

(D) Schematic diagram of diffusion and permeation within the spatial model. Cells and cell walls were built up from 0.5 µm square grid points, the minimum unit in the model. Arrows indicate diffusion or permeation between each grid point. For the parameters that were used in the simulations, see Table 1-1.

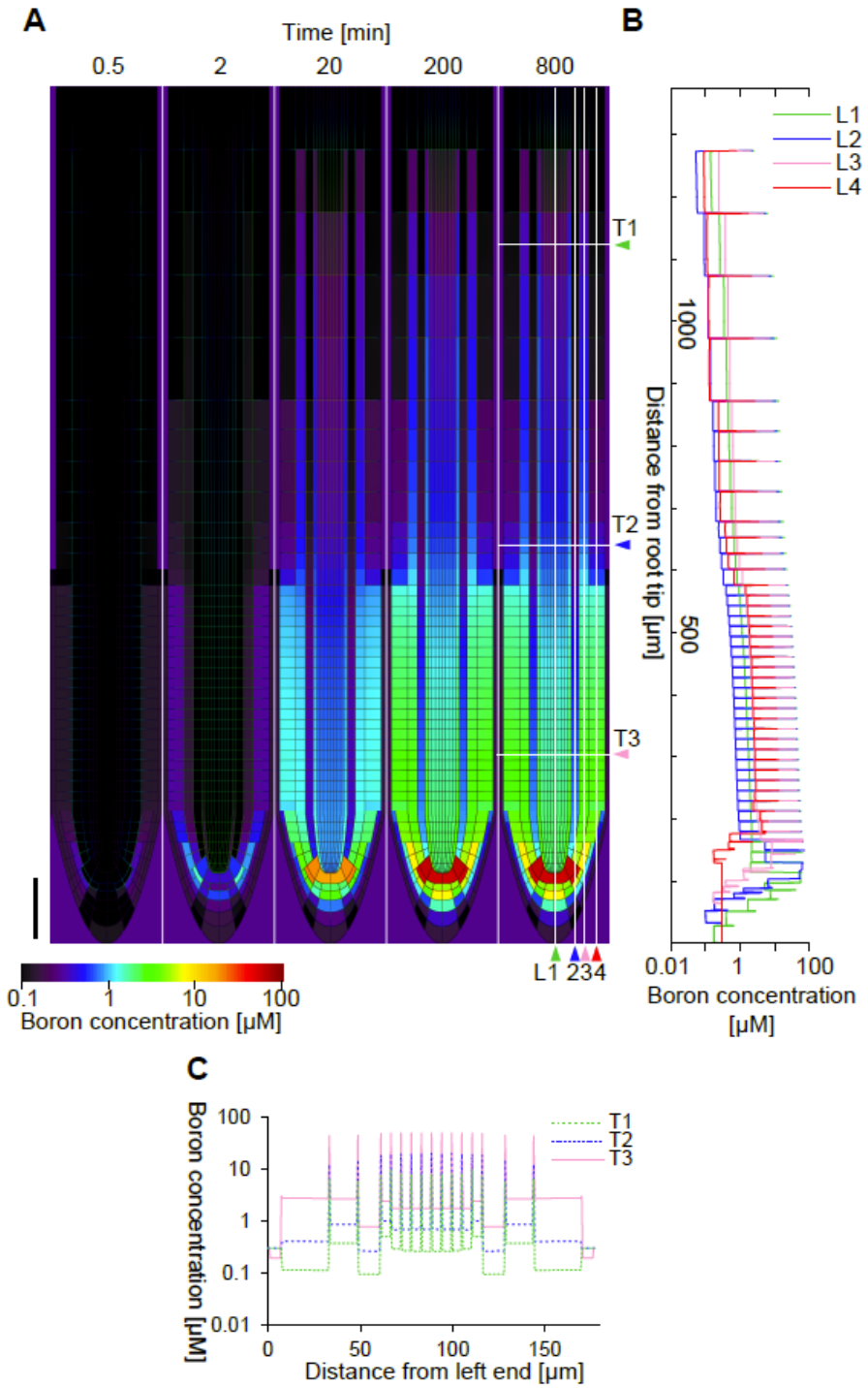

Figure 1-2 Simulation of boron distribution in roots

In the simulation the root whose initial boron content was zero was immersed into a 0.3 μM boron medium. The simulation was run for 480,000 time steps, corresponding to 800 min of the immersion. (A) Frames depict the temporal change in the spatial distribution of boron after the immersion. After 200 min the distribution pattern no longer changed. Scale bar, 100 μm. Boron profiles in longitudinal (L1-4) and transversal (T1-3) sections are also shown by line graph in (B) and (C), respectively.

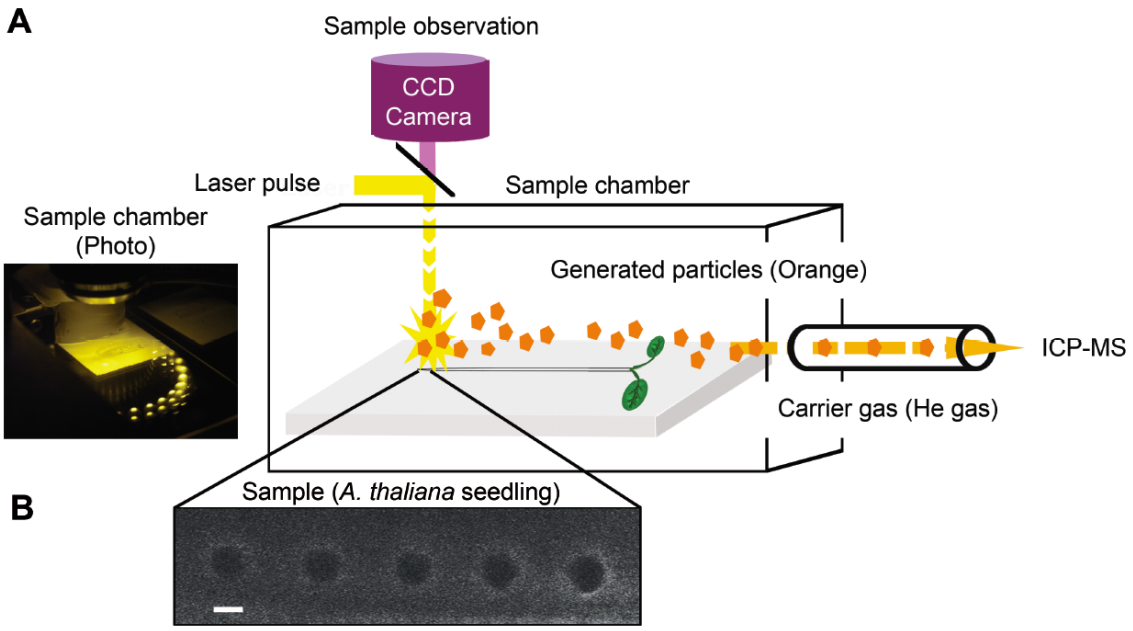

Figure 1-3 Workflow of LA-ICP-MS analysis. (A) *A. thaliana* five-day-old seedlings were placed in the chamber of the laser ablation apparatus. Observation through the CCD camera was used to select the position of the spots to be ablated. A laser beam of 10 µm in diameter was applied to the root, and ablated materials (orange) were drawn into the ICP-MS by the carrier He gas. (B) A picture of *A. thaliana* roots after three rounds of ablation at the same positions. Dark circles represent the sampling spots of the laser ablation. The settings for spot diameter and spot spacing were 10 µm and 30 µm, respectively. Scale bar,10 µm.

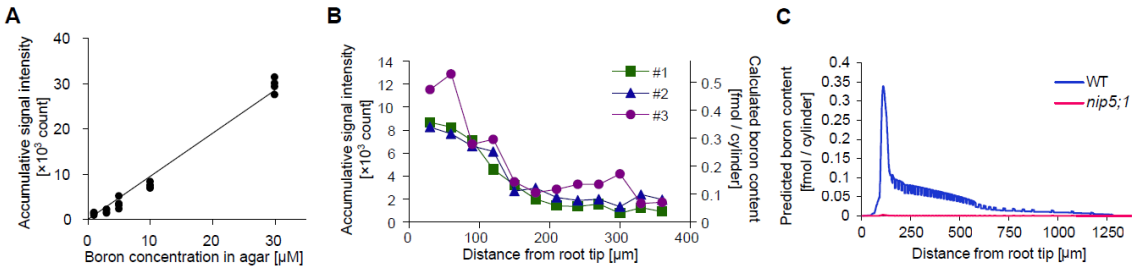

Figure 1-4 Quantitative analysis of boron distribution in *A. thaliana* roots by LA-ICP-MS.

(A) Calibration curve for LA-ICP-MS. Data points and the linear regression line are shown. The slope of the linear regression and the volume of the ablated cylinder in the LA-ICP-MS allowed to calculate a quantitative link between the count and the boron content: "boron content [fmol]" =4 × 10^{-5} × "accumulative signal intensity [count]". The coefficient of determination was 0.986. (B) Signal count of LA-ICP-MS and calculated boron content in the ablated cylinder at various positions from the tip of the root. Profiles obtained from three independent wild-type seedlings are shown. Note that any detectable signal was not obtained from *nip5;1* mutant even though same position in root tip was ablated.(C) Predicted boron content when LA-ICP-MS would be applied to the *in silico* root, integrated over a 10 μm diameter at each position in the root at the 800 min time point.

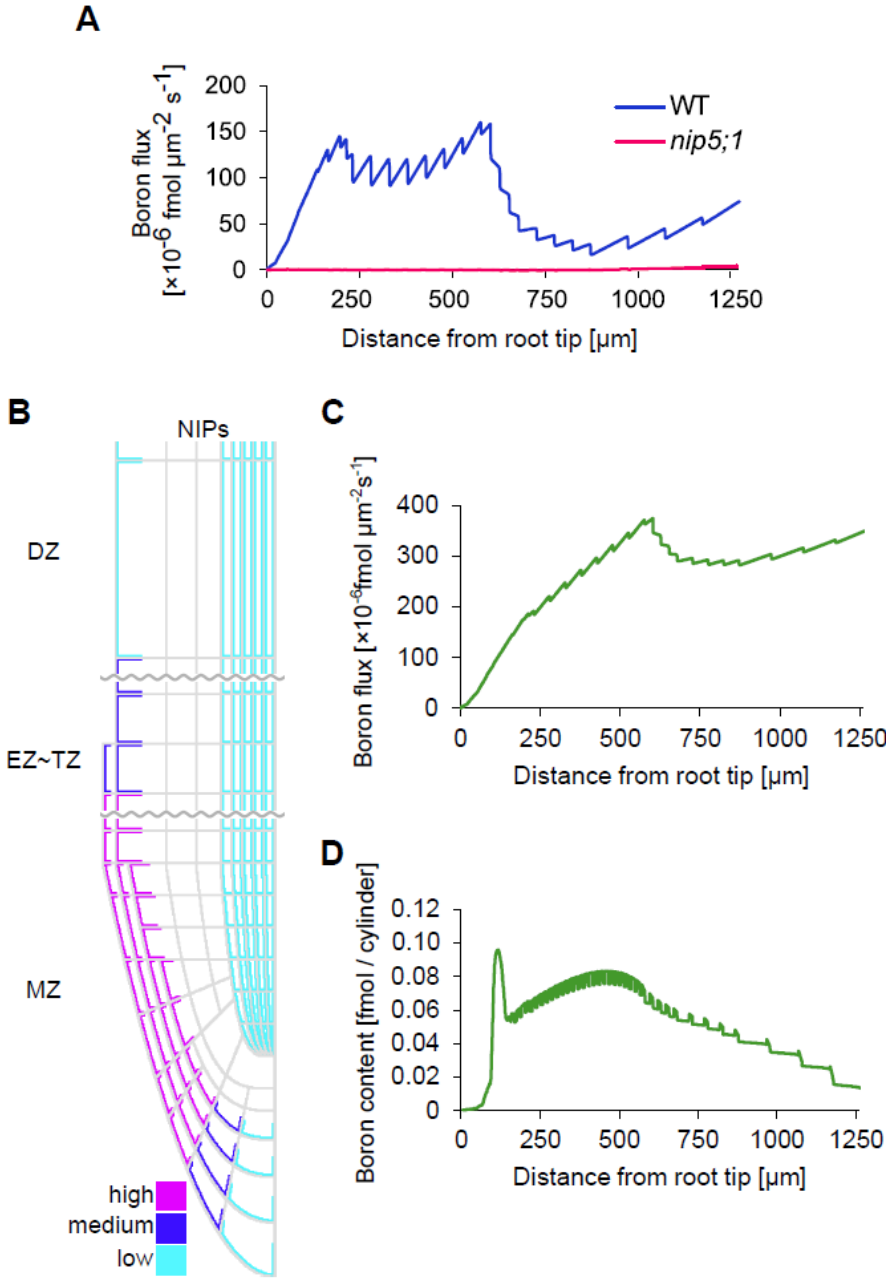

Figure 1-5 Mathematical modelling analysis of the flux affected by NIPs in stele.

Simulations of a root whose initial boron content is zero, immersed into a 0.3 µM boron medium. Simulations were run for 480,000 time steps, corresponding to 800 min. (A) Net shootwards boron flux for each longitudinal position along the root at the 800 min time point. (B) Layout of NIPs in the modified model. NIPs with low permeability were introduced into the stele and pericycle, with the intention to enhance upward boron flux. The layout of BORs used in the model was identical to that of Figure 1-1B. (C) Net shootwards boron flux for each longitudinal position along the root at the 800 min time point. (D) Boron content as predicted by the modified model, in case LA-ICP-MS would be applied to the *in silico* root.

Table

Table 1-1 Parameters for simulation

Symbol	Description	Value			Unit
Δt	Time step	0.1			s
Δx	Space step	0.5			μm
D_{cy}	Boron diffusion constant in cytosol	1100			$\mu m^2 s^{-1}$
D_{cw}	Boron diffusion constant in cell wall	73.3			$\mu m^2 s^{-1}$
p_m	Membrane permeability of boron	0.01			$\mu m\, s^{-1}$
Symbol	**Description**	**High**	**Medium**	**Low**	**Unit**
p_{NIP}	Boron permeability facilitated by NIP	1.5	0.6	0.3	$\mu m\, s^{-1}$
p_{BOR}	Boron efflux permeability facilitated by BOR	1.5	0.6	0.3	$\mu m\, s^{-1}$

Table 1-2 Parameters settings for LA-ICP-MS used in this study

Laser ablation instrumentation	NWR-193X (ESI)
Laser type	ArF (wavelength 193 nm)
Carrier gas	He
Laser power	5 mJ
Spot diameter	10 μm
Frequency of laser pulse applied	5 Hz
Wash-out time	5 s
Laser irradiation time per spot (dwell time)	5 s
Pulse duration	5 ns
Time interval between spots	20 s
Carrier gas flow	600 ml min^{-1}

Chapter2.

Rapid transporter regulation prevents substrate flow traffic jams — a case study of boron transport

本章の内容は、学術雑誌論文として出版する計画があるため公表できない。5 年以内に出版予定。

Chapter3.

A possible role of NADPH oxidase *RBOHC* in response to excess boron stress in *Arabidopsis thaliana*

本章の内容は、学術雑誌論文として出版する計画があるため公表できない。5 年以内に出版予定。

Chapter4.

A mutation in *ANAC103* alleviates DNA damage in *Arabidopsis thaliana* mutant sensitive to excess boron.

本章の内容は、学術雑誌論文として出版する計画があるため公表できない。5 年以内に出版予定。

Chapter5.

TPR5 is involved in directional cell division and is essential for the maintenance of meristem cell organisation in *Arabidopsis thaliana*

Declaration

The research described in this chapter was conducted in collaboration with Drs. Lukram Shantikumar, Takuya Sakamoto, Sachihiro Matsunaga, under the supervision of Toru Fujiwara, and the portions of the studies conducted by the co-authors are indicated in the subtitles. Some of the experiments were performed with technical assistance from Mses. Yayoi I. Tsujimoto and Yuko Kawara. Some figures are from in Naoyuki Sotta's master thesis, which are declared in each figure legend.

Abstract

Root growth in plants is achieved through the coordination of cell division and expansion. In higher plants, the radial structure of roots is formed during embryogenesis and maintained thereafter throughout development. Here we show that the tetratricopeptide repeat domain protein *TPR5* is necessary for maintaining radial structure and growth rates in *Arabidopsis thaliana* root. We isolated an *A. thaliana* mutant with reduced root growth and determined that *TPR5* was the gene responsible for the phenotype. The *tpr5-1* mutant root growth rate was reduced to ~60% of that in wild-type plants. The radial structure was disturbed by the occurrence of occasional extra periclinal cell divisions. While the number of meristematic cells was reduced in the *tpr5* mutants, the cell length in the mature portion of the root did not differ from that of the wild type, suggesting that TPR5 is required for proper cell division but dispensable for cell elongation. Expression of the TPR5-GFP fusion protein driven by the *TPR5* promoter displayed fluorescence in the cytoplasm of root

meristems, but not in mature root regions. DNA staining revealed that frequencies of micronuclei were increased in root meristems of *tpr5* mutants. Through this study, we concluded that *TPR5* is involved in preventing formation of micronuclei, and is necessary for both the activity and directionality of cell division in root meristems.

Introduction

The roots of *Arabidopsis thaliana* display radial cellular organisation arranged in the order of stele, endodermis, cortex and epidermis cells from the inside to the outside (Dolan et al., 1993). The fundamental structure is conserved through the roots, enabling continuous root elongation and efficient substance transport. Root elongation is achieved by both cell elongation in the elongation zone and cell proliferation in proximal meristems. The size of the proximal meristem is conserved during postembryonic development via a balance between cell proliferation and differentiation (Beemster et al., 1998). In root meristems, the quiescent centre (QC) renders the surrounding cells as stem cells and forms a stem cell cluster, which is called the stem cell niche and includes the stele initials, pericycle initials, cortex/endodermis initials (CEI) and epidermis/lateral root cap initials (van den Berg et al., 1997). The stem cells undergo asymmetric cell division to produce self-renewing cells and daughter cells (Dolan et al., 1993). Whereas daughter cells derived from stele and pericycle initials undergo symmetric cell division, CEI daughter cells divide asymmetrically resulting in a cortex cell and endodermal cell couplet. Likewise, the epidermis/lateral root cap initial daughter cells divide into epidermal cells and lateral root cap cells. These daughter cells detach from stem cell niches and undergo several rounds of symmetric, longitudinal division before transiting from the proximal meristems to the transition zone and losing their cell division activity (reviewed by Perilli et al., 2012). During cell proliferation, it is critical to maintain the cell division planes perpendicular

to the elongating axis; otherwise, the radial structure will not be maintained.

Several genes are involved in the proper alignment of the cell division plane, and mutation of diverse genes involved in the establishment of the division site results in mis-positioned cell plates (Reviewed by Müller, 2012) *TONNEAU2*/*FASS* is a putative regulator of protein phosphatase A2, which is necessary for pre-prophase band (PPB) assembly, and its mutants exhibit cell division planes in random orientations (Traas et al., 1995; Camilleri et al., 2002). *TONNEAU1* interacts with centrin and is essential for PPB formation (Azimzadeh et al., 2008). TANGLED and RanGAP, whose depletion results in disorganised root cell files, is concentrated at the PPB and remains associated with the cortical division site (Xu et al., 2008; Walker et al., 2007). The mitogen-activated protein kinase MPK6, which is localised in the PPB and phragmoplast, is involved in control of the cell division plane during early development (Müller et al., 2010). Mutants of PHRAGMOPLAST ORIENTING KINESIN 1 and 2 exhibit improper placement of cell walls (Müller et al., 2006). Although these extensive studies have revealed the mechanisms of cell division plane alignment (reviewed by Müller, 2012), gaps in our understanding of these complex mechanisms remain.

Here we report the identification and characterisation of a novel player in *Arabidopsis thaliana* root patterning, the tetratricopeptide repeat (TPR) domain protein TPR5. While the TPR domain is known to interact with other proteins to form complexes (Lamb et al., 1995), to our knowledge, there have been no studies on the involvement of *TPR5* in any biological processes. We demonstrated that *tpr5* mutants exhibited slower root elongation, disordered radial root cell organisation with misplaced cell division planes, and decreased numbers of meristematic cells. In addition, we demonstrated that *TPR5* is expressed in root meristems throughout the cell cycle and is necessary for preventing micronuclei formation.

Materials and Methods

Plant materials and growth conditions

The B13.4/*tpr5-1* mutant was selected from a Col-0 *gl1-1* ethylmethane sulfonate irradiated M_2 population (Lehle seeds, USA), and *tpr5-2* (SALK099949) was obtained from the Arabidopsis Biological Resource Center. The T-DNA homozygous line was established using the PCR primers SALK099949_LP and SALK099949_RP (Table 5-S1).

Wild-type (Col-0) or mutant seeds were surface-sterilised for 1 min with 70% ethanol and for 1 min with 99% ethanol. After removing the ethanol, the seeds were sown on sterilised MGRL (Fujiwara et al., 1992) plates supplemented with 1% sucrose, solidified with 1.5% gellan gum, and then incubated at 4°C for 2 days. Plates were placed vertically in incubators at 22°C under a 16-h light: 8-h dark cycle.

Reverse transcription-polymerase chain reaction (RT-PCR)

Total RNA was prepared from whole roots of 15-day-old seedlings with RNeasy Plant Mini Kit (Qiagen) according to the manufacturer's instructions. Approximately 500-ng total RNA were used for reverse transcription with Prime Script RT Master Mix (Takara, Japan) according to the instructions using the 10-µL scale. The product was diluted tenfold and used as PCR templates. For semi-quantitative RT-PCR, the *TPR5* coding sequence and *Actin8* were amplified by three-step PCR with Go taq Green Master Mix (Promega). The PCR conditions were as follows: denaturation at 95°C for 2 min, then 31 cycles of three steps, 95°C for 30 s, 55°C 30 s and 72°C 20 s (90 s for *TPR5*), followed by extension at 72°C for 7 min. Primer sets TPR5_CDS_F (and _R) or ACTIN8_RT_F (and _R) were used (Table 5-S1). Quantitative RT-PCR of *CYCB1;1* was performed with SYBR® *Premix Ex Taq*™ II (Tli RNaseH Plus, Takara) based on the protocol provided by the manufacturer. *Actin8* was used as an internal control and primer sets CYCB1;1_RT_F (and _R) or

ACTIN8_F (and _R) were used (Table 5-S1).

Positional identification of the responsible gene

For genetic linkage analysis, the F_2 generation was obtained from a cross between B13.4 (Col-0 background) and L*er*. Single sequence length polymorphism (SSLP) and single nucleotide polymorphism (SNP) markers between Col-0 and L*er* were used to detect the genotype. Genetic markers near the candidate region are shown in Table 5-S2.

Root length measurement and counting of lateral root number

Seedlings on medium plates were photographed using a Canon EOS Kiss digital camera and images were saved using JPEG. The root length was measured from the digital images using the segmented line mode of the ImageJ software (http://rsbweb.nih.gov/ij/). The number of emerged lateral roots was counted via observation under a stereomicroscope.

Generation of transgenic plants

For the complementation test, either genomic or coding DNA sequences (CDS) were introduced into *tpr5-2*. For the genomic sequence line, the promoter region and open reading frame excluding the stop codon were amplified from the genomic sequence by PCR with the primers TRP5_pro_F and TPR5_CDS_R. For the CDS line, the coding sequence excluding the stop codon was amplified from cDNA using TPR5_fuse_F and TPR5_CDS_R primers. The promoter region was amplified with primer TPR5_pro_F and TPR5_fuse_R. These fragments were mixed and fused using PCR, and amplified with the TRP5_pro_F and TPR5_CDS_R primers. The DNA fragments were introduced into pENTR / D-TOPO vector (Invitrogen) and transferred into pMDC107 vector (Curtis and Grossniklaus, 2003) using the gateway LR clonase recombination system (Invitrogen).

To generate the promoter-GUS line, the promoter region of *TPR5* was cloned into the pENTR / D-TOPO vector using primers TPR5_pro_F and TPR5_pro_R, and transferred into the pMDC162 vector (Curtis and Grossniklaus, 2003) using the gateway LR clonase recombination system.

The binary vectors were introduced into *Agrobacterium tumefaciens* strain GV3101 (Bechtold and Pelletier, 1998) and *tpr5-2* (for the complementation test) or Col-0 (for promoter-GUS analysis) plants were transformed with these cultures using the floral dipping method (Clough and Bent, 1998). The transformed plants were selected on half strength MS medium containing 20 μg/mL hygromycin B (Wako) and 250 μg/mL Claforan (Sanofi, Japan), solidified with 0.5% agarose.

GUS staining

Seedlings were vacuum infiltrated with GUS staining solution comprising 100 mM Na_2HPO_4 buffer pH 7.0, 0.1% Triton X-100, 2 mM $K_3Fe[CN]_6$, $K_4Fe[CN]_6$ and 0.5 mg mL^{-1} X-GlcA (5-bromo-4-chloro-3-indolyl-β-D-glucuronide cyclohexyl ammonium salt, Wako, Japan) for 15 min at room temperature and incubated at 37°C in the dark for 16 h. Whole seedlings were photographed using a Canon Eos Kiss digital camera. For detailed observation by microscopy, stained seedlings were clarified by overnight incubation with chloral hydrate solution (4-g chloral hydrate, 1-mL glycerol, and 2-mL water) on microscope slides and observed under an optical microscope with bright field for Fig. 5 C and E, or differential interference contrast for Fig. 5 A, D, F and G .

Confocal microscopy

For observation of the cell wall, roots were cut and mounted on a slide glass with 10 μg/mL PI solution and observed after 15 min. Fluorescence from PI was observed using a confocal laser

scanning microscope FV1000 or FV1200 (Olympus). The wavelengths for excitation and emission were 559 nm and 570-670 nm, respectively. For observation of GFP fluorescence of transgenic plants, roots were mounted with water and observed using 473 nm and 510 nm for excitation and emission, respectively. For DNA staining, roots were fixed in 4 % (w/v) formaldehyde in PBS (137 mM NaCl, 2.68 mM KCl, 8.1 mM Na_2HPO_4·1.47 mM KH_2PO_4) for 10 min at 4°C. After washed with PBS, the fixed roots were stained with 4',6-diamidino-2-phenylindole (DAPI) using the staining buffer of CyStain® UV Precise P DNA staining kit for 2 min at room temperature. Stained samples were washed and mounted with PBS. DAPI signal was detected under confocal microscopy with wavelength 405 nm and 461 nm for excitation and emission, respectively.

Assessment of cell cycle stages

For the detection of cells in S phase, seedlings 3 days after germination (DAG) were placed in liquid medium containing half strength-MGRL and 10 μM 5-ethynyl-2'-deoxyuridine (EdU) in Click-iT component A (Invitrogen) for 30 min at 22°C under continuous light. EdU incorporation was stopped by fixation with 4% PFA/PBS for 30 min under vacuum. After three washes with PBS, the seedlings were incubated with 0.5% Triton X-100/PBS for 20 minutes. After three washes with PBS, EdU was labelled with Alexa flour 594 azide following the manufacturer's instructions. Nuclei were stained with SYBR Green I (Lonza) diluted 5,000-fold with 0.5% Triton X-100/PBS for 10 min. The seedlings were then mounted with 1/2 × mounting medium as described in Hayashi et al. (2013). Fluorescence emitted from Alexa flour 594 and SYBR Green I was observed using a fluorescent microscope (IX-81, Olympus) equipped with a confocal scanning unit (CSUX-1, Yokogawa) and a sCMOS camera (Neo 5.5 sCMOS ANDOR Technology). The excitation and emission wavelengths were 561 nm and 604-644 nm for EdU and 488 nm and 503-537 nm for SYBR Green I, respectively. Images were analysed using ImageJ software. M phase cells were distinguished from others cells

based on SYBR Green I staining, with obvious features of prophase, metaphase, anaphase and telophase.

Results

Slow root elongation and small shoots of the B13.4 mutant

Declaration: Isolation of B13.4 mutant was conducted by Dr. Takuya Sakamoto and Yuko Kawara.

We isolated an *A. thaliana* mutant by screening for mutants defective in root growth. The phenotype was confirmed in the M_3 generation, and the mutant line was termed B13.4 (Fig. 1A). B13.4 carried a single recessive mutation responsible for the phenotype. To characterise root growth of B13.4 in detail, we measured the root length of the mutant almost every day up to 9 DAG. The primary root length of B13.4 was about two thirds that of the wild type throughout the growth period (Fig. 1B). Assuming constant growth rates of the roots, the average growth rate of B13.4 was 61% of that in the wild type. Although B13.4 appeared to develop fewer lateral roots at 7 DAG (Fig. 1A), microscopic observation revealed that the number of emerged lateral roots per primary root length did not differ significantly between wild type and B13.4 (Fig. 1C). B13.4 exhibited smaller shoots compared to wild type (Fig. 1D)

Decreased cell number in B13.4 root meristem

The root growth rate was determined by meristem activity and cell expansion (Beemster et al., 1998). To evaluate the meristem activity, we estimated the cell number in root meristems. The meristematic zone was defined as the area between the QC and the first elongating cortex cell. To quantitatively

estimate the boundary between the meristem and the elongation zone, we measured the lengths of all cortex cells from the QC to the elongation zone in 3 DAG seedlings. The data suggested that the average cell length starts to increase at the 24th and 35th cells from the QC in B13.4 and the wild type, respectively (Fig. 2A). The different positions of the initiation of cell elongation indicate that the number of meristematic cells was reduced in B13.4.

To compare the final lengths of the root cells, we measured the cell length in the mature region of B13.4 and wild-type roots. No significant difference was observed in the mature cell length between B13.4 and wild-type roots (Fig. 2B).

Perturbation in the radial structure and occasional cell death in B13.4

Propidium iodide (PI)-stained seedlings were observed at 3 DAG using a confocal microscope. The cellular organisation in the root meristems differed between the wild type and B13.4 (Fig. 2C, D). In B13.4, the cell files in the root meristems were partially disordered with the occurrence of non-canonical pericrinal cell divisions (Fig. 2D, arrowheads). These pericrinal cell divisions were observed with higher frequency in the cortex, endodermis and epidermis cells compared to the wild type (Table 5-1). These extra cell files were observed locally and discontinued from each initial, suggesting that these defective patterns were not caused by abnormal periclinal cell division of stem cells. In addition, PI-stained dead cells were observed with higher frequency in the epidermis, cortex, endodermis and stele of B13.4 compared with the wild type (Fig. 2D, asterisk; Table 5-2).

Identification of TPR5 as the causal gene for the short root phenotype of B13.4

Declaration: Identification of the causal gene and generation of plant materials were conducted by Drs. Lukram Shantikumar, Takuya Sakamoto and Yayoi I. Tsujimoto.

To identify the causal gene for the root growth defect in B13.4, we conducted map-based cloning. B13.4 (Col-0 background) was crossed with L*er*, and its F_2 population was used for genetic mapping. Molecular genetic analysis of 501 individual F_2 plants was performed using Col-0 and L*er* genetic markers, and the B13.4 locus was mapped to a 32-kb region on BAC clone F13N6 on chromosome 1 in a region that contained eight predicted genes (Fig. 3A). The genomic sequences of the region corresponding to the open reading frames of the eight genes were determined, and only one mutation was found in *TPR5* (AT1G56440) with no mutations in the other genes. The mutation was located in the 3′ end of the fifth intron in a predicted splicing acceptor site (Fig. 3B). The nucleotide sequence of the B13.4 *TPR5* mRNA was determined by RT-PCR, and sequence analysis revealed that splicing of the fifth intron of *TPR5* occurred improperly in B13.4. The *TPR5* mRNA contained an additional 20 bp in the mutant (Fig. 3C, D), establishing that intact TPR5 protein was not produced in B13.4.

To confirm that the mutation in *TPR5* caused the B13.4 phenotype, we obtained a tagged line allele with T-DNA insertion in *TPR5*, and isolated a line with the homozygous T-DNA insertion. We detected no intact *TPR5* transcript in the tagged line (Fig. 3C), and the allele exhibited similar defects in root growth (Fig. 4A, B) and radial organisation (Fig. 4C) to B13.4. We designated B13.4 and the T-DNA allele as *tpr5-1* and *tpr5-2*, respectively. In addition, we conducted a complementation experiment by expressing a TPR5-GFP fusion protein under the control of the 5′ upstream region of *TRP5* (1.6 kb upstream region from the start codon) in *tpr5-2*. We constructed two types of *TPR5-GFP* fusion proteins, one with genomic *TPR5* and the other with *TPR5* CDS. For each construct, we obtained two independent transformants homozygous for T-DNA insertion in the T_3 generation. All homozygous lines generated were tested for their growth, and all lines recovered root elongation (Fig. 4B). In addition, root radial organisation was recovered in both lines (Fig. 4C, D, Table 5-1, 2).

TPR5 promoter activity observed mainly in stele and QC, but not in proximal meristem cells

Declaration: The plant materials were generated by Drs. Lukram Shantikumar and Takuya Sakamoto.

To investigate the tissue specificity of the *TPR5* promoter activity, we generated Col-0 background transgenic plants expressing the *β-glucuronidase* (GUS) reporter gene under the control of the 1.6-kb *TPR5* promoter region, which was identical to the fragment used in the complementation test. We generated eight independent transformants, and staining of their T_2 generation revealed that seven of the eight lines exhibited similar staining patterns. Here we describe one of the representative transgenic plants among the seven lines.

Seedlings at 1 DAG were GUS-stained to observe the expression patterns in early stages. GUS staining was observed in cotyledons, hypocotyls and roots. In roots, strong staining was observed in stele (Fig. 5A). At 8 DAG, staining was observed mainly in the vascular tissue in both roots and shoots with strong staining in young leaves (Fig. 5B). In the primary roots, GUS staining was observed mainly in the stele, QC and several cells surrounding the QC (Fig. 5B, C, D). Weak or no GUS staining was detected in the cell division zone other than the QC region (Fig. 5C, E), where the defect in cell division occurs in *tpr5* mutants (Fig. 2 D).

No GUS staining was observed in the tips of emerged lateral roots (Fig. 5F). On the other hand, GUS staining was observed in the columella of the elongated lateral roots, but not in the proximal meristem (Fig. 5G).

TPR5-GFP fusion protein was localised mainly in root meristems

Declaration: The plant materials were generated by Drs. Lukram Shantikumar and Takuya

Sakamoto.

We investigated TPR5 protein localization using TPR5 (genomic)-GFP fusion in the transgenic *tpr5-2* lines used for the complementation test (Fig. 4). Driven by its own promoter, TPR5-GFP fusion showed the strongest fluorescence in the meristems in these transgenic plants, which became weaker towards the elongation zone and columella cells (Fig. 6 A–C). Higher magnification revealed strong and uniform signal near the cell periphery, which was absent from the central portion of the cells (Fig. 6 D–F), suggesting cytoplasmic localization of the fusion protein. In mature regions of the roots, significant GFP fluorescence was not observed (Fig. 6 G–I).

To further investigate the expression of TPR5 during each cell cycle stage, we visualized DNA by DAPI staining and observed TPR5-GFP localization in meristematic epidermal cells (Fig. 7). During interphase and prophase of cell division, TPR5-GFP was observed in cytosol but not inside nuclei. From metaphase to telophase, TPR5-GFP was uniformly localized in cells including the area where chromosomes were observed.

Micronuclei were frequently observed in tpr5 mutants

Declaration: Observation of micronuclei and EdU incorporation assay was conducted by Takuya Sakamoto.

The aberrant cell division and cell death in *tpr5* mutant root meristems motivated us to consider the possibility of cell cycle disruption. Nuclei of 3 DAG root meristems were stained with SYBR Green I (Fig. 8A and B, green signal), which revealed that 73.7% (n=19) of *tpr5-1* and 72.2% (n=18) of *tpr5-2* seedlings had at least one cell with micronuclei (Fig. 8C) in longitudinal confocal sections of root meristems, whereas no micronuclei were observed in any wild type seedlings (n=17). The

frequency of cortical cells with micronuclei were 0% (n=1380) in wild type, 2.8% (n=1159) in *tpr5-1* and 1.9 % (n=1165) in *tpr5-2*, that suggested defects in chromosomal separation in the *tpr5* mutants. To obtain a further hint on the possible involvement of TPR5 in cell cycle progression, we visualised nuclei during the DNA synthesis phase by pulse labelling using the thymidine analog EdU and calculated the percentage of cortical cells in M or S phase in confocal sections of root meristems. Both *tpr5-1* and *tpr5-2* exhibited slightly but significantly higher proportions of mitotic cells (Fig S1A), whereas those in S phase did not differ significantly between *tpr5* mutants and wild type (Fig S1B). Quantitative RT-PCR revealed that *CYCB1;1* mRNA, whose accumulation is specific to G2-to-M transition (Shaul et al., 1996) , was accumulated in roots of *tpr5* mutants significantly higher than in wild type (Fig S1C). These results suggest involvement of TPR5 in cell cycle progression.

Discussion

Involvement of TPR5 in root meristem maintenance through cell division

The root elongation rate was reduced in the B13.4/*tpr5-1* mutant, compared with the wild type (Fig. 1), whereas the cell length of the mature portion of the root remained unchanged (Fig 2B). Considering the reduction in meristematic cell numbers in the B13.4/*tpr5-1* mutant, the slower root elongation in this mutant is due to reduced root meristem activity, which should be explained by disturbed cell cycle progression and/or reduced number of cell cycling in meristems. Increased portion of cortical meristem cells in M phase and increased *CYCB1;1* mRNA accumulation in *tpr5* mutants (Fig S1) indicate that cell cycle progression is disturbed in *tpr5* mutants. In consideration of the fact that micronuclei were observed at a higher frequency in *tpr5* mutants, TPR5 is likely to be involved in chromosomal separation, since micronuclei formation is often coincident with malfunction in mitotic events, namely, a defective anaphase checkpoint, dysfunctional spindle or

defects in the kinetochore (reviewed by Fenech et al., 2011). TPR5-GFP signal was observed throughout the cell cycle. During mitosis, the TPR5-GFP signal overlapped DAPI signal representing chromosomal location (Fig. 7), suggesting that TPR5 can participate in any of those processes related to micronuclei formation. The frequently observed abnormal direction in the cell division plane in *tpr5* mutants suggests that TPR5 is involved in determination of cell division plane. From these results we conclude that *TPR5* is necessary for both activity and directionality of cell division in root meristems, which is indispensable for constant cell production and maintenance of the elaborate radial structure of the root.

TPR5 was reported to harbour three TPR domains (Prasad et al., 2010). The TPR domain is a protein-protein interaction domain first identified in a study of the cell cycle regulator *CDC23* (Sikorski et al., 1990). Thereafter, proteins containing TPR domains were found in diverse biological processes such as transcription repression, stress response, protein kinase inhibition, mitochondrial and peroxisomal protein transport and neurogenesis (reviewed by Goebl et al., 1991; D'Andrea et al., 2003). To our knowledge, there has been no report on the involvement of *TPR5* in any developmental processes or on its enzymatic activity.

It is well known that SCARACROW (SCR) regulates periclinal cell division in CEI daughter cells (Di Laurenzio et al., 1996), which suggests *TPR5* involvement in the regulation by SCR. However, ectopic expression analysis of SCR in *scr-4* revealed that activation of SCR in ground tissue induced periclinal division, but no effect was detected when SCR was expressed in other tissues, establishing that SCR acts cell-autonomously to control asymmetric cell division only within ground tissue (Heidstra et al., 2004). In the case of *tpr5* mutants, cell division in an abnormal direction was not cell file-specific and not continuous from the stem cells (Table 5-1 and Fig 2D). Hence, it cannot be assumed that altered expression of SCR is the cause of the non-canonical periclinal cell division observed in *tpr5* mutants. That observation also implies that TPR5 is involved

in general cell division functions, rather than in the determination of cell identity.

A similar situation with *tpr5* mutants has been reported in *TONSOKU/MGOUN3/BRUSHY1* mutants, which is involved in stabilisation of chromatin structure (Guyomarc'h et al., 2004; Suzuki et al., 2004; Takeda et al., 2004). Those mutants exhibit root growth defects and oblique cell division in root meristems, although the length of fully expanded cells is comparable to that of the wild type. Those mutants accumulate cells expressing *CYCB1;1:GUS* in shoot and root apical meristems, suggesting that cell cycle progression at the G2/M phase is important for regulating cell division patterns during plant development (Suzuki et al., 2005; Inagaki et al., 2006). It was reported that *TONSOKU/MGOUN3/BRUSHY1* interacts with TSK-associating protein 1 (TSA1) through the LGN motif, which is categorised as a TPR motif subfamily, and their involvement in mitosis has been suggested (Suzuki et al., 2004). As in *TONSOKU/MGOUN3/BRUSHY1*, it is likely that TPR5 participates in some protein complexes that function in cell division. Identification of the interactors is a further subject of study.

Tissue specificity of TPR5 expression

The *TPR5* promoter activity was observed mainly in steles and around QCs but not in proximal meristems (Fig. 5). In contrast, fluorescence of TPR5-GFP fusion protein was observed in whole root meristems, including the region where extra periclinal cell division and cell death were observed (Fig. 6). It is possible that the coding region of *TPR5* harbours elements essential for expression in the meristem, or there might be a non-cell-autonomous function via movement of *TPR5* mRNA or protein. Although the mechanisms for the discrepancy between tissues with promoter activity and the GFP fusion protein remain unknown, we can conclude that the TPR5 protein is expressed and functions in root meristems judging from the spatial concordance between localization of the fusion protein and observed meristem phenotype.

Acknowledgments

We thank Yayoi T. Inui and Yuko Kawara for technical assistance. We also acknowledge support and helpful comments from Yoshihiro Ohmori, Koji Kasai and Akie Shimotohno. This work was supported in part by the Japan Society for the Promotion of Science [Grant-in-Aid for Scientific Research number 21228002 to T.F.]

Tables

Table 5-1. Proportions of seedlings in which extra periclinal cell divisions were observed.

	Extra periclinal cell divisions (%)			
	En	Cor	Epi	n
Col-0	6.45	3.23	0	31
tpr5-1	37.1	42.9	11.4	35
tpr5-2	56.5	43.5	17.4	23
tpr5-2 TPR5-GFP	0	0	0	12

Meristem zones in 3-day-after-germination seedlings were observed. Values are expressed as percentages of seedlings in which at least one extra periclinal cell division was observed. *tpr5-2 TPR5-GFP* is genetically identical to *tpr5-2 TPR5*(genomic)-*GFP* L1 in Fig. 4. En, endodermis; Cor, cortex; Epi, epidermis; n, the number of seedlings analysed.

Table 5-2. Proportions of seedlings in which dead cells were observed.

	Dead cells (%)				
	En	Cor	Epi	St	n
Col-0	3.23	0	0	6.45	31
tpr5-1	2.86	31.4	62.9	74.3	35
tpr5-2	13.0	52.2	69.6	56.5	23
tpr5-2 TPR5-GFP	0	0	0	0	12

Meristem zones of 3-day-after-germination seedlings were observed. Values are expressed as percentages of seedlings in which at least one extra periclinal cell division was observed. *tpr5-2 TPR5-GFP* is genetically identical to *tpr5-2 TPR5*(genomic)-*GFP* L1 in Fig. 4. En, endodermis; Cor, cortex; Epi, epidermis; St, Stele; n, the number of seedlings analysed.

Table 5-S1. Primers used in this study

Name	Sequence
TPR5_pro_F	CACCATGGATGGCACACAGGGAAC
TPR5_CDS_R	CTGTTTAAGGCAGTATCTTGAC
TPR5_pro_R	TCTGAGAGAGATTCTCCGGCGAGC
TPR5_CDS_F	CACCATGGCTAGGTCACCGAGCAAAC
TPR5_fuse_F	CGGAGAATCTCTCTCAAATGGCTAGGTCACCGAGC
TPR5_fuse_R	GCTCGGTGACCTAGCCATTCTGAGAGAGATTCTCCG
Actin8_RT_F	GCCAGATCTTCATCGTCGTG
Actin8_RT_R	TCTCCAGCGAATCCAACCTT
CYCB1;1_RT_F	TAAGCAGATTCAGTTCCGGTCAAC
CYCB1;1_RT_R	GGGAGCTTTACGAAAGAAATACTCC
SALK099949_LP	CATTTCTGTCAGAAGGCTTCG
SALK099949_RP	CAGAAGAAGTTCAATGAGGCG

Table 5-S2. Genetic markers near the *tpr5-1* mutation used in map-based cloning

Maker	Forward	Reverse	Type
T22H22	TTTATCAGCTCCTGCATGCTT	AAAAGAAGAGAGGGAGGCTCA	SSLP
F13N6_1	CATACCTCGACGCACAGCTA	TTCATTTCATCCATCGCAGA	SNP
F13N6_2	GAAGCTGGACGAGGATGAAG	AGCGGGAAAATAAAGCAGGT	SSLP
F13N6_3	TTGTTGGGATTGGGAAAAAC	CGGGATAACGCGATTTAGTG	SSLP
F23H11	GGTTTGATGGAGATTTTGCTG	GGGATATTGCTGCAAAGGAA	SSLP

Figures

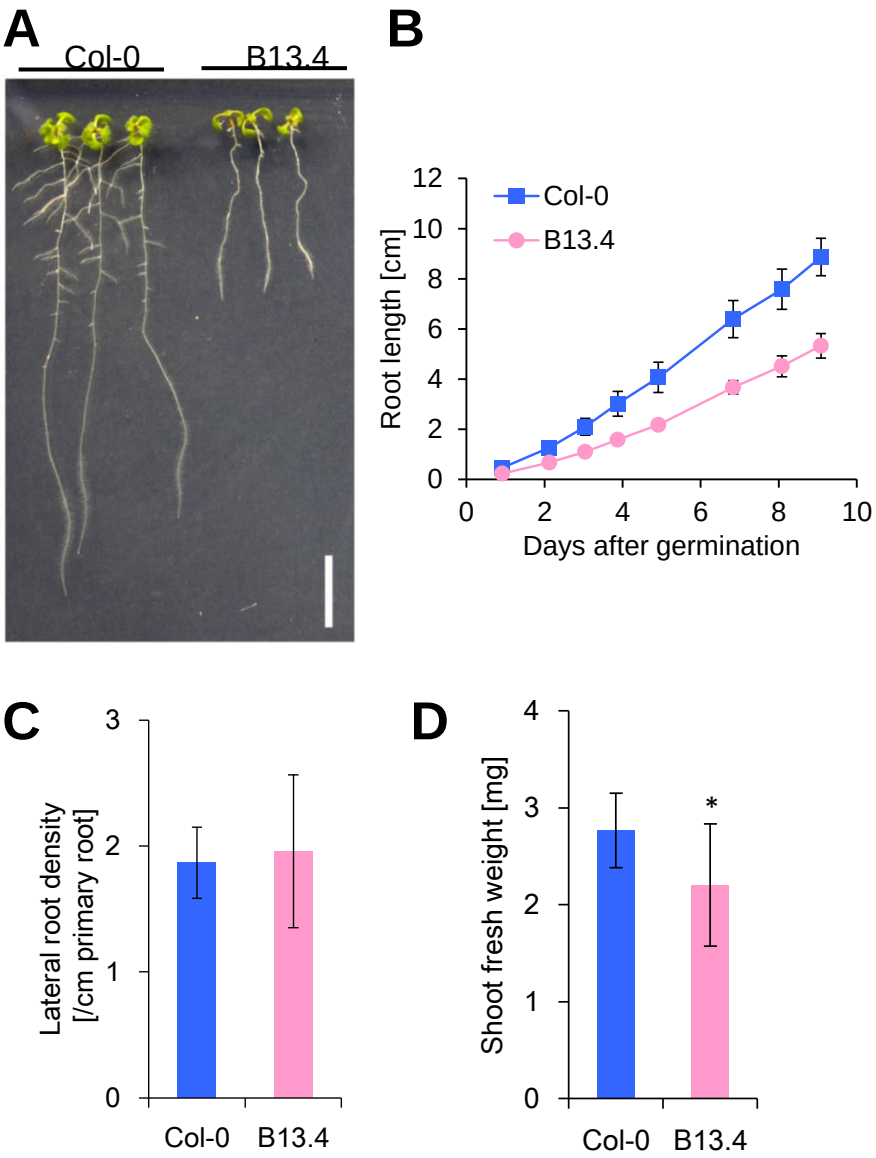

Fig. 1. Growth of the B13.4 mutant. (A) Seven DAG seedlings from the wild type and B13.4 mutant grown on MGRL plates. Bar, 1 cm. (B) Time course of root length-change in the wild type and B13.4 mutant after germination. Values represent the mean ± standard deviations of 14-19 measurements. (C) Lateral root density per primary root length. Lateral root number of 7-DAG seedlings was counted using stereomicroscopy. No significant difference was detected between Col-0 and B13.4 by Welch's *t*-test at $p < 0.05$. n=15-16 seedlings. (D) Shoot fresh weight measurement of the 7-DAG wild type and B13.4 mutant. Values represent the mean ± standard deviations of 11-20 measurements. Asterisks indicate a significant difference from Col-0 at $p < 0.05$ by Welch's t-test. *A and B are from the master thesis*

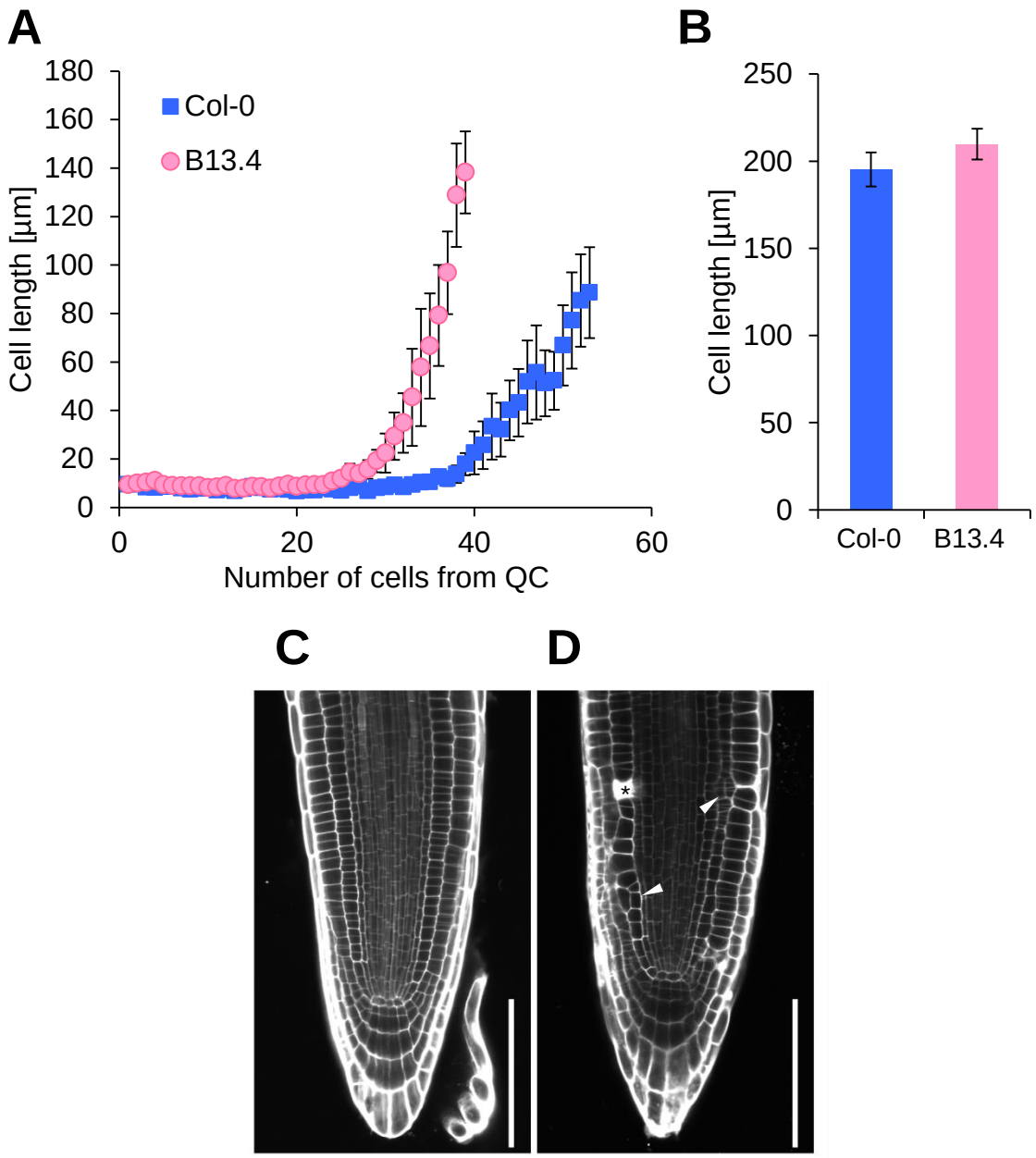

Fig. 2. Root cell organisation of B13.4. (A) Longitudinal cell length of each cortex cell in root meristem of 3 DAG seedlings. Cell numbers were counted from the quiescent centre. Values are the mean ± standard error of measurements from 10 seedlings. (B) Longitudinal length of mature cortex cells in 3 DAG wild type and B13.4. Values represent the mean ± standard errors of at least 60 measurements from 10 individual seedlings. (C and D) Confocal images of 3 DAG wild-type (C) and B13.4 (D) roots stained with PI. Arrowheads indicate extra periclinal cell divisions, and an asterisk indicates dead cells stained with PI. Bars, 100 µm. *A is from the master thesis, modified.*

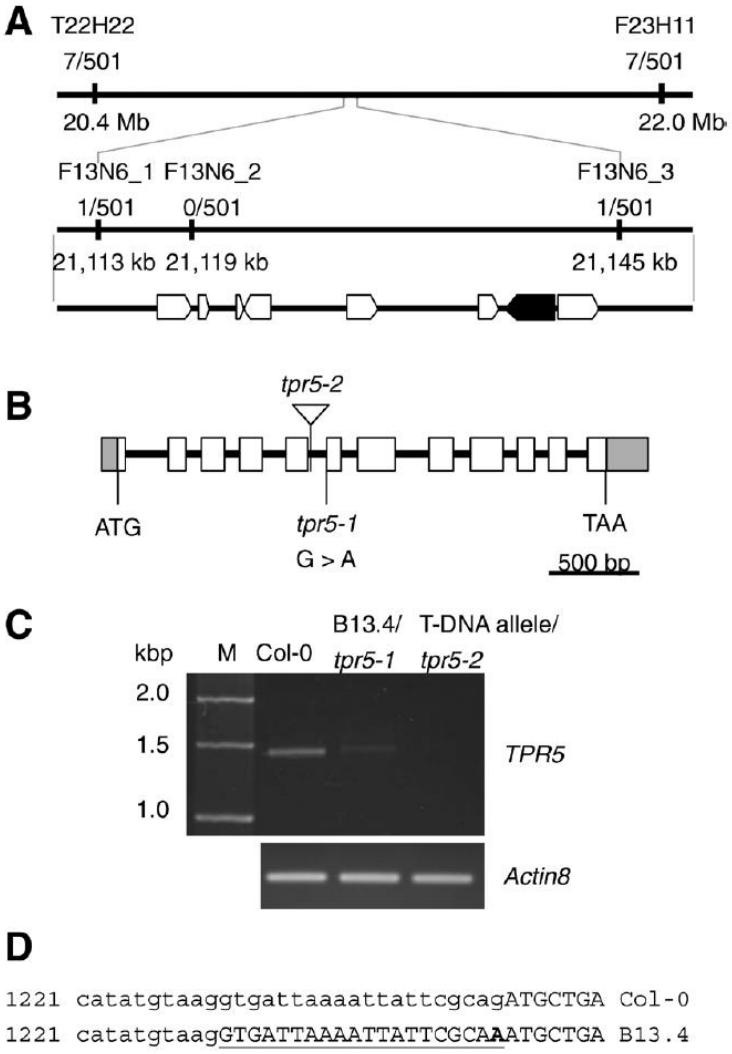

Fig. 3. Positional identification of the mutation responsible for B13.4. Molecular markers and the number of recombinant plants found in the mapping population are shown. (A) Marker position and predicted genes in mapped region. Eight candidate genes selected by the map-based cloning are indicated at the bottom. The gene in which a mutation was found is filled in black. (B) Exon-intron structure of *TPR5* and positions of mutations in *tpr5* alleles. Rectangles and bars represent exons and introns, respectively. UTRs are filled in grey. T-DNA insertion is indicated by a triangle. (C) *TPR5* transcripts in *tpr5* mutants. Total RNA was prepared from whole roots of 15-day-old seedlings, and *TPR5* coding sequence and *Actin8* were amplified by RT-PCR. M, DNA size marker. (D) Altered splicing site of *TPR5* in B13.4. *TPR5* genomic sequences around the fifth intron are shown. Exons and introns are represented by upper and lower case, respectively. The numbers on the left side indicate base pair positions from annotated transcription start site in TAIR10 annotation. The mutation in B13.4 is indicated in bold and extra exon is underlined. Note that the extra 20 bp exon causes a shift in the reading frame. *From the master thesis, modified.*

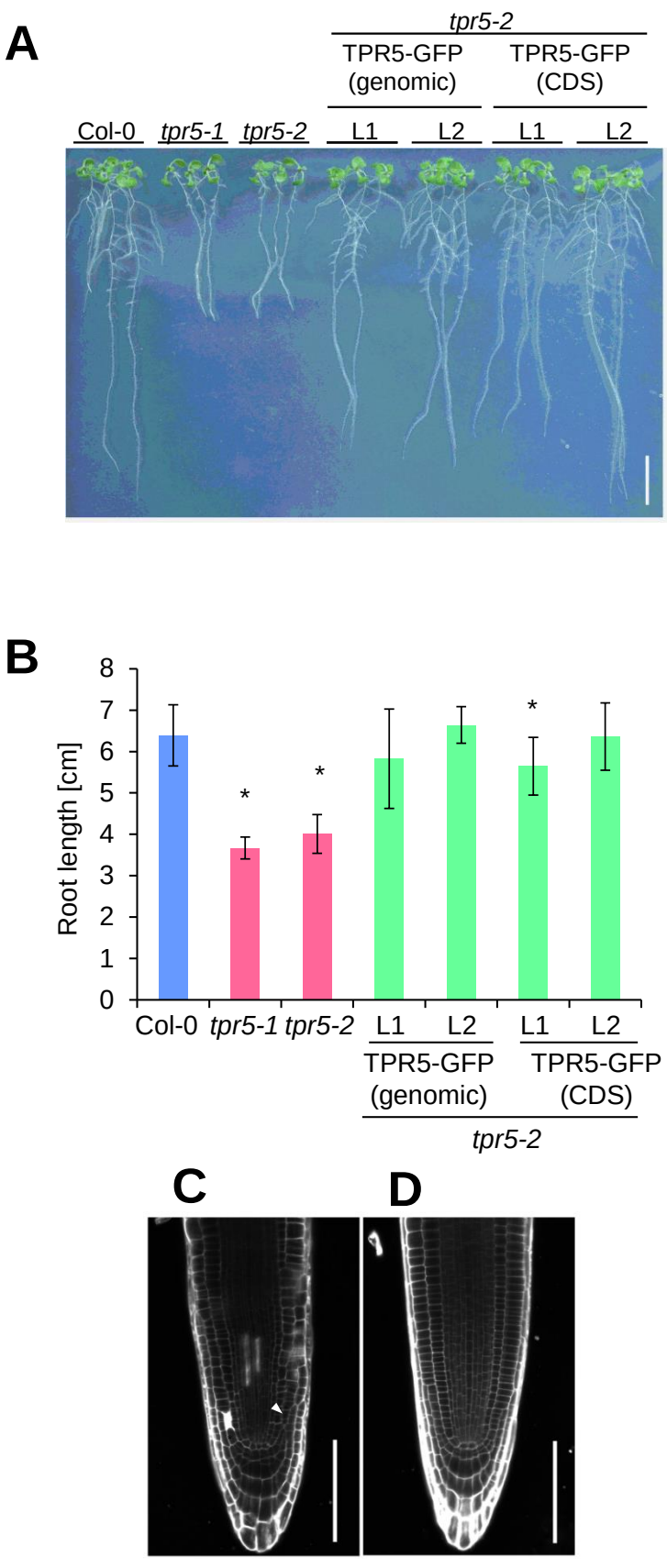

Fig. 4. Complementation test for *tpr5-2*. (A) Root growth phenotype of *tpr5-2* complementation lines. The *tpr5-2* mutant was transformed with a GFP-fused TPR5 genomic or cDNA sequence driven by its 1.6-kbp promoter. Seven DAG seedlings are shown. Bar = 1 cm. (B) Root growth measurement of *tpr5* mutants and complementation lines. Primary root lengths of 7 DAG seedlings were measured. Values are means ± standard deviation of 14-19 seedlings. Asterisks indicate significant differences from Col-0 at $p < 0.05$ by Welch's *t*-test. L1 and L2 represent independent transgenic plants for each construction. (C and D) Confocal images of 3 DAG roots of *tpr5-2* (C) and *tpr5-2 TPR5* (genomic)-*GFP* L1 (D) stained with PI. Arrowheads indicate extra periclinal cell divisions, and an asterisk indicates dead cells stained with PI. Bars = 100 µm.

A and B are from the master thesis, modified.

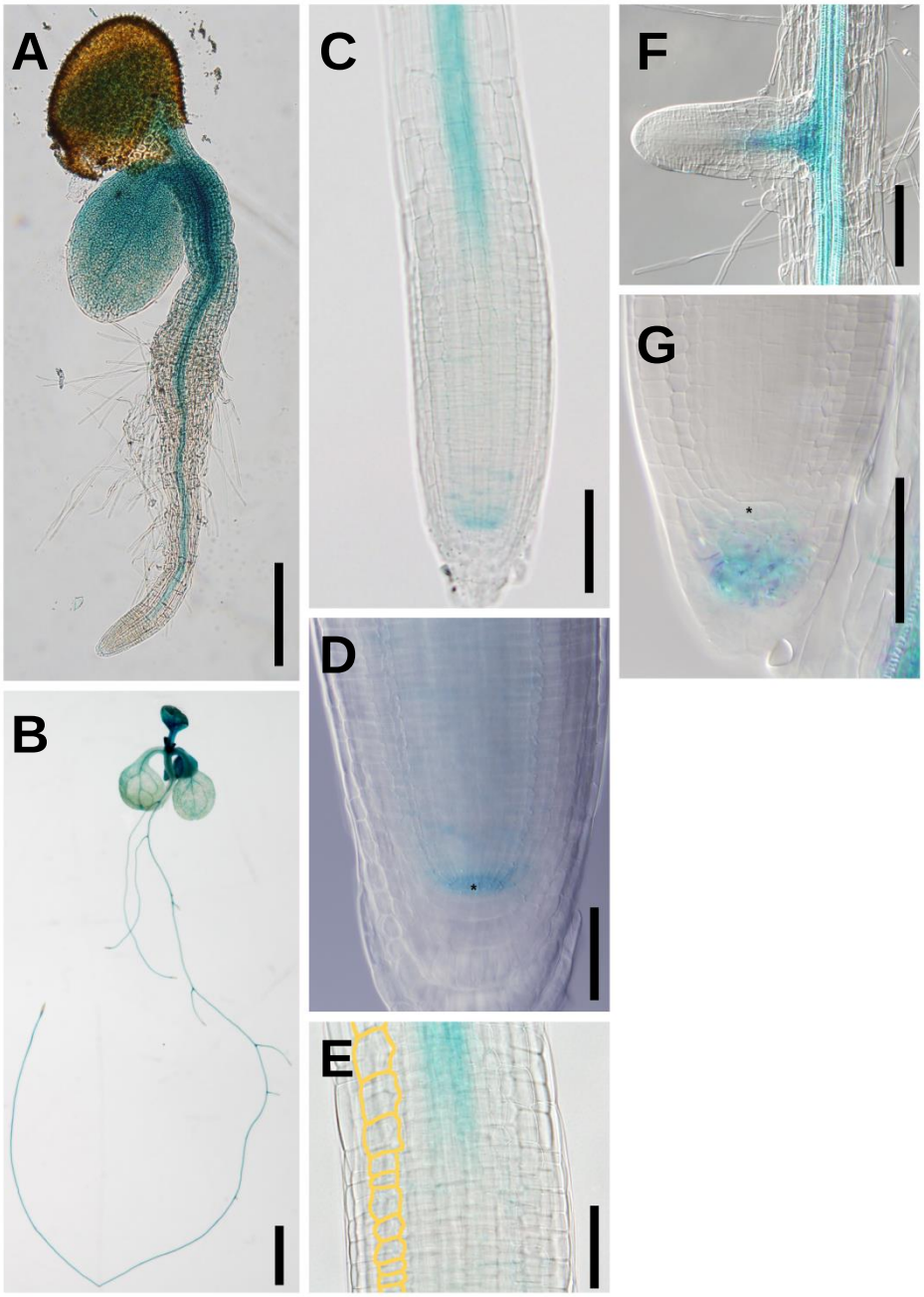

Fig.5. *TPR5* promoter-GUS expression patterns. Representative expression patterns of 1 DAG (A) and 8 DAG seedlings (B-G) are shown. (A) Whole seedling at 1 DAG. (B) Whole seedling at 8 DAG. (C) Primary root tip. (D) Close-up view of the meristem in primary root. Asterisk indicates QC cell position. (E) Close-up view of elongation zone in primary root. A cell file in the cortex is highlighted by orange. (D) (F) Emerged lateral root. (G) Root tip of mature lateral root. Asterisk indicates QC cell position. Bars: A, C, F 100μm; B, 2 mm; D, E, G 50 μm.

B is from the master thesis.

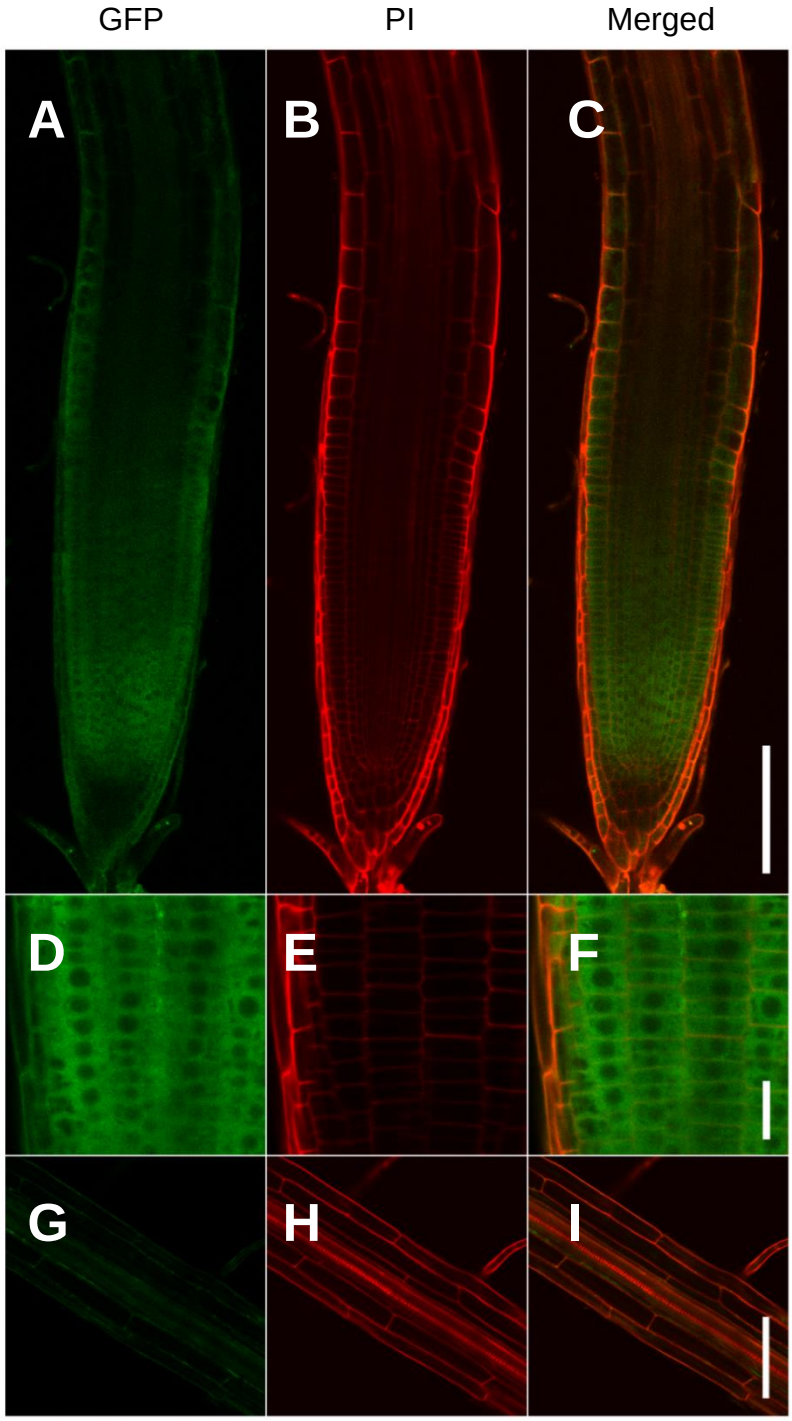

Fig. 6. Tissue specific expression of TPR5-GFP fusion protein. Three DAG seedlings of transformants expressing TPR5-GFP (genetically identical to *tpr5-2 TPR5*(genomic)-*GFP* L1 in Figure 5-4) were observed using confocal microscopy. The cell wall was stained with PI. (A-C) Representative images of primary root tips. (D-F) Primary root tips with higher magnification. (G-I) Mature region with root hair. Bars: A-C, G-I 100 μm; D-F 20 μm.

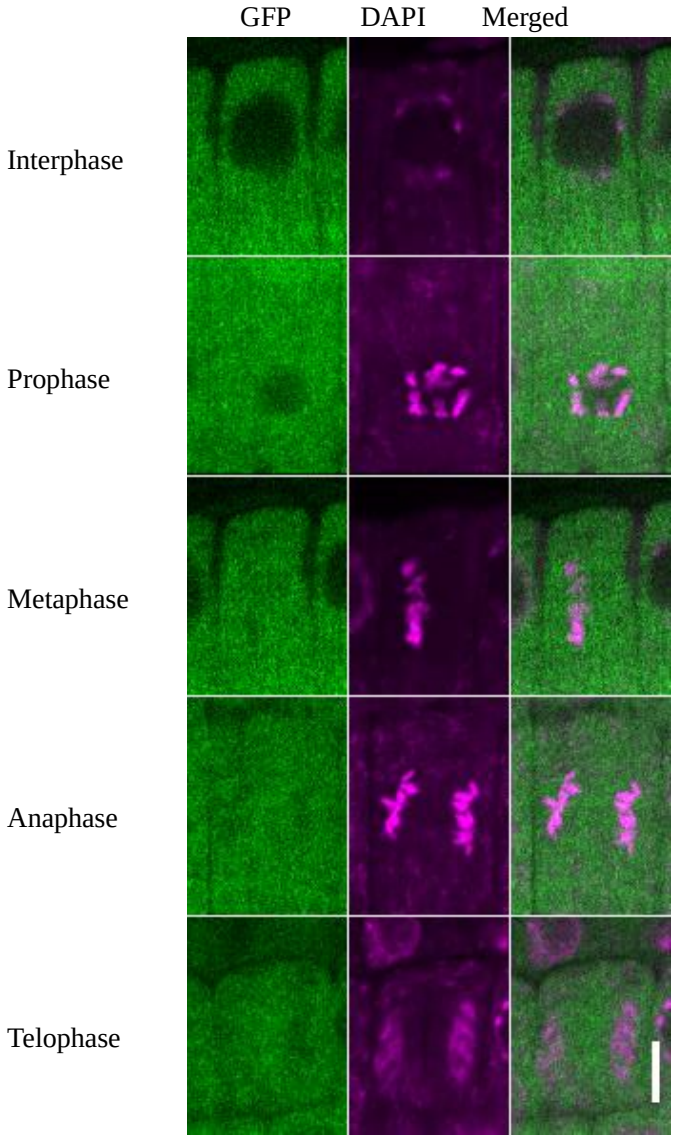

Fig. 7. Subcellular localization of TPR5-GFP fusion protein during cell division.

Three DAG seedlings of transformants expressing TPR5-GFP (genetically identical to *tpr5-2 TPR5*(genomic)-*GFP* L1 in Figure 5-4) were observed using confocal microscopy. DNA was stained with DAPI and root meristematic epidermal cells in each cell division phase were observed. Bar: 5 μm.

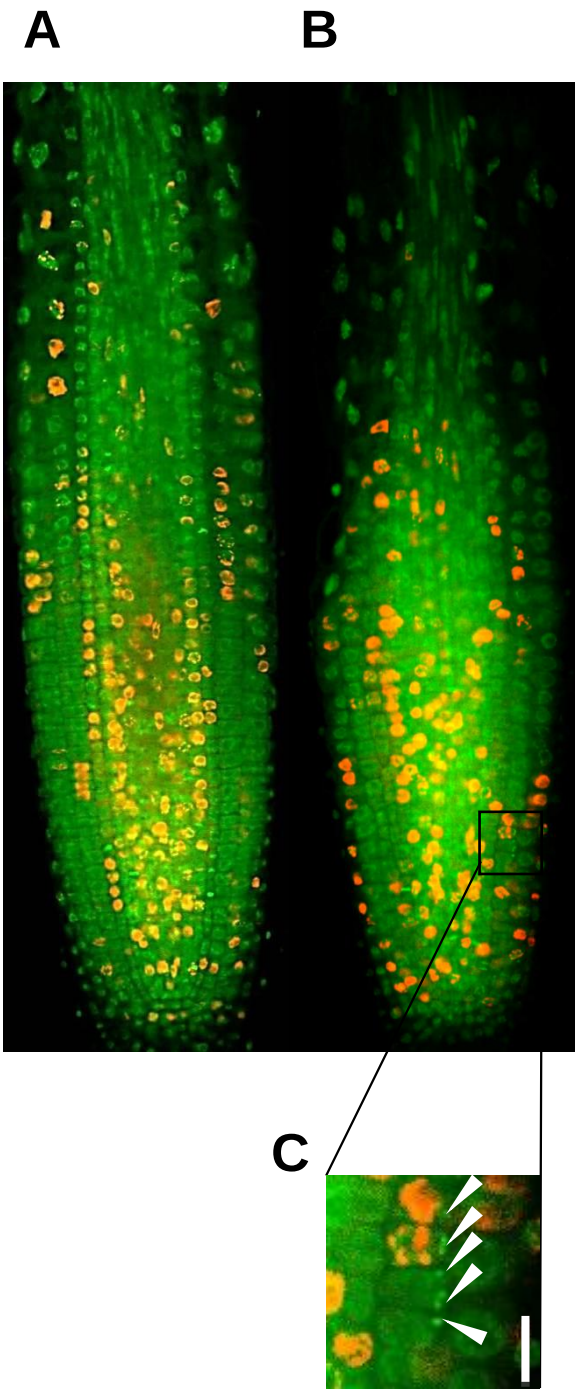

Fig. 8. Micronucleus formation in *tpr5* mutants. In root meristems of 3 DAG seedlings, nuclei were visualised by SYBR green I staining, and nascent DNA was labelled by pulse treatment with EdU for 30 minutes. Representative patterns of nuclei (SYBR Green I, green) and nascent DNA (EdU, red) are shown for wild type (A) and *tpr5-1* (B). Bars: 100 μm (C) Magnification of a part of image (B) representing cortex cells having micronuclei (arrowheads). Bars: 10 μm.

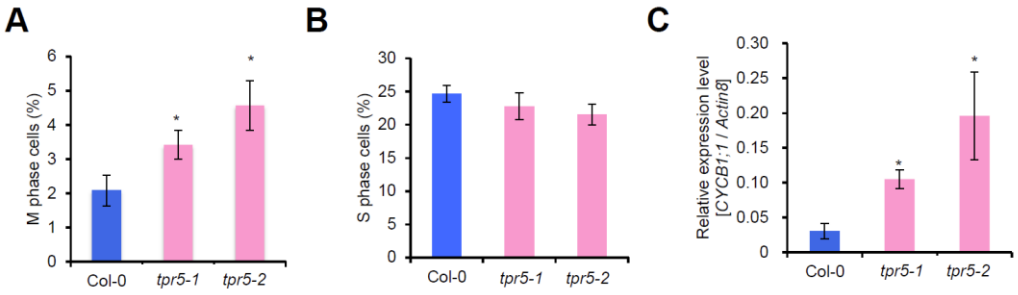

Fig. S1. Proportions of the cortical cells in M or S phase in *tpr5* mutants
(A) Proportion of cortex cells showing any mitotic features (prophase, metaphase, anaphase and telophase). Asterisks indicate a significant difference from Col-0 at p < 0.05 by Welch's *t*-test. (B) Proportion of S phase cells in the cortex. Values in (A) and (B) are the mean ± standard errors of 17–19 seedlings. There was no significant difference between wild type and each mutant at *p*> 0.05 by Welch's *t*-test. (C) mRNA accumulation of CYCB1;1 in *tpr5* mutants. mRNA was extracted from roots of 15 day-old seedlings and *CYCB1;1* mRNA accumulation was determined by qRT-PCR. Expression levels are normalized by that of *Action8* and expressed in the mean ± standard errors of three biological replication. Asterisks indicate a significant difference from Col-0 at *p* < 0.05 by Welch's *t*-test.

Conclusions

In this thesis, I have extended our knowledge on boron as a nutrient, in distinct views of its transport and physiological functions. The mathematical model established in Capter1 successfully predicted boron gradient through roots which were confirmed by LA-ICP-MS analysis. The models predicted discontinuously increasing flux from root tips toward shoots, which provided us with the novel idea that root tips and other parts have distinct function in boron uptake: Root tips are responsible for boron uptake for root growth, and the other parts are for boron to send to shoots. Importantly, the model will be the foundation of further modeling for more complex models, namely with transporter regulation, cell growth or hormonal signaling to chapter the unobvious behavior of the system. Another mathematical model to study boron transporter regulation in Chapter2, demonstrated that the swift regulation of boron transporters, which appears to be much swifter than they needs to be at a first glance, is crucial for preventing unitability of the system. This work not only provided us with explanation for the significance of swift regulation of boron transporters, but demonstrated the general nature of transport systems consists from substrate-regulated facilitators and exporters with opposite polarity. In Chapter3, I presented evidences which suggest that NACPH oxidase *RBOHC* should be responsible for the root growth inhibition under excess boron stress. In Chapter4, I identified transcription factor *NAC103* as a determinant of excess-boron induced ROS production, DNA damage and growth defects under the absence of a proteasome component *RPT5A*, suggesting the importance of controlling NAC103 expression through Ub-proteasome pathway for excess boron tolerance. In addition to those findings, in Chapter5, I identified an uncharacterized gene *TPR5*, which is essential for root meristem maintenance and cell division in roots. Throughout these achievements, I have acquired mathematical approaches for analyzing dynamics of non-linear systems, and programming skills to realize that. Together with experiences on conducting experiments on genetics and molecular biology to test hypothesis, I have established the foundation

for integrated study from multiple perspectives to any subjects.

References

Amor, Y., Babiychuk, E., Inzé, D., & Levine, A. (1998). The involvement of poly (ADP ‐ribose) polymerase in the oxidative stress responses in plants. *FEBS Letters, 440*(1-2), 1-7.

Aquea, F., Federici, F., Moscoso, C., Vega, A., Jullian, P., Haseloff, J., & ARCE ‐JOHNSON, P. (2012). A molecular framework for the inhibition of arabidopsis root growth in response to boron toxicity. *Plant, Cell & Environment, 35*(4), 719-734.

Ardıc, M., Sekmen, A. H., Turkan, I., Tokur, S., & Ozdemir, F. (2009). The effects of boron toxicity on root antioxidant systems of two chickpea (cicer arietinum L.) cultivars. *Plant and Soil, 314*(1-2), 99-108.

Arrigo, A., Tanaka, K., Goldberg, A. L., & Welch, W. J. (1988). Identity of the 19S'prosome'particle with the large multifunctional protease complex of mammalian cells (the proteasome).

Audetat, A., Gunther, D., & Heinrich, C. A. (1998). Formation of a magmatic-hydrothermal ore deposit: Insights with LA-ICP-MS analysis of fluid inclusions. *Science (New York, N.Y.), 279*(5359), 2091-2094.

Azimzadeh, J., Nacry, P., Christodoulidou, A., Drevensek, S., Camilleri, C., Amiour, N., . . . Bouchez, D. (2008). Arabidopsis TONNEAU1 proteins are essential for preprophase band formation and interact with centrin. *The Plant Cell, 20*(8), 2146-2159. doi:10.1105/tpc.107.056812 [doi]

Battich, N., Stoeger, T., & Pelkmans, L. (2015). Control of transcript variability in single mammalian cells. *Cell, 163*(7), 1596-1610.

Bechtold, N., & Pelletier, G. (1998). In planta agrobacteriummediated transformation of adult arabidopsis thaliana plants by vacuum infiltration. *Arabidopsis protocols* (pp. 259-266) Springer.

Beemster, G. T., & Baskin, T. I. (1998). Analysis of cell division and elongation underlying the developmental acceleration of root growth in arabidopsis thaliana. *Plant Physiology, 116*(4), 1515-1526.

Camilleri, C., Azimzadeh, J., Pastuglia, M., Bellini, C., Grandjean, O., & Bouchez, D. (2002). The arabidopsis TONNEAU2 gene encodes a putative novel protein phosphatase 2A regulatory subunit essential for the control of the cortical cytoskeleton. *The Plant Cell, 14*(4), 833-845.

Cervilla, L. M., Blasco, B., Rios, J. J., Romero, L., & Ruiz, J. M. (2007). Oxidative stress and antioxidants in tomato (solanum lycopersicum) plants subjected to boron toxicity. *Annals of Botany, 100*(4), 747-756. doi:mcm156 [pii]

Chen, P., & Umeda, M. (2015). DNA double‐strand breaks induce the expression of flavin‐containing monooxygenase and reduce root meristem size in arabidopsis thaliana. *Genes to Cells, 20*(8), 636-646.

Chi, P., Ko, F., Hsu, C., Chen, H., Yang, C., Sun, Y., & Yang, M. (2002). Direct impurity analysis of semiconductor photoresist samples with laser ablation ICP-MS. *Journal of Analytical Atomic Spectrometry, 17*(4), 358-365.

Ciechanover, A. (1994). The ubiquitin-proteasome proteolytic pathway. *Cell, 79*(1), 13-22.

Ciechanover, A. (1998). The ubiquitin-proteasome pathway: On protein death and cell life. *The EMBO Journal, 17*(24), 7151-7160. doi:10.1093/emboj/17.24.7151 [doi]

Clough, S. J., & Bent, A. F. (1998). Floral dip: A simplified method forAgrobacterium‐mediated transformation ofArabidopsis thaliana. *The Plant Journal, 16*(6), 735-743.

Cools, T., Iantcheva, A., Weimer, A. K., Boens, S., Takahashi, N., Maes, S., . . . De Veylder, L. (2011). The arabidopsis thaliana checkpoint kinase WEE1 protects against premature vascular differentiation during replication stress. *The Plant Cell, 23*(4), 1435-1448. doi:10.1105/tpc.110.082768 [doi]

Cruz-Ramírez, A., Díaz-Triviño, S., Blilou, I., Grieneisen, V. A., Sozzani, R., Zamioudis, C., . . . Dhonukshe, P. (2012). A bistable circuit involving SCARECROW-RETINOBLASTOMA integrates cues to inform asymmetric stem cell division. *Cell, 150*(5), 1002-1015.

Culligan, K. M., Robertson, C. E., Foreman, J., Doerner, P., & Britt, A. B. (2006). ATR and ATM play both distinct and additive roles in response to ionizing radiation. *The Plant Journal, 48*(6), 947-961.

Curtis, M. D., & Grossniklaus, U. (2003). A gateway cloning vector set for high-throughput functional analysis of genes in planta. *Plant Physiology, 133*(2), 462-469. doi:10.1104/pp.103.027979 [doi]

Czechowski, T., Stitt, M., Altmann, T., Udvardi, M. K., & Scheible, W. R. (2005). Genome-wide identification and testing of superior reference genes for transcript normalization in arabidopsis. *Plant Physiology, 139*(1), 5-17. doi:139/1/5 [pii]

da Silva, Marcelo Anselmo Oseas, & Arruda, M. A. Z. (2013). Laser ablation (imaging) for mapping and determining se and S in sunflower leaves. *Metallomics, 5*(1), 62-67.

D'Andrea, L. D., & Regan, L. (2003). TPR proteins: The versatile helix. *Trends in Biochemical Sciences, 28*(12), 655-662.

Dannel, F., Pfeffer, H., & Römheld, V. (1998). Compartmentation of boron in roots and leaves of sunflower as affected by boron supply. *Journal of Plant Physiology, 153*(5), 615-622.

Dixit, V., Pandey, V., & Shyam, R. (2001). Differential antioxidative responses to cadmium in roots and leaves of pea (pisum sativum L. cv. azad). *Journal of Experimental Botany, 52*(358), 1101-1109.

Dolan, L., Janmaat, K., Willemsen, V., Linstead, P., Poethig, S., Roberts, K., & Scheres, B. (1993). Cellular organisation of the arabidopsis thaliana root. *Development (Cambridge, England), 119*(1), 71-84.

Dunand, C., Crèvecoeur, M., & Penel, C. (2007). Distribution of superoxide and hydrogen peroxide in arabidopsis root and their influence on root development: Possible interaction with peroxidases. *New Phytologist, 174*(2), 332-341.

Duncan, S., Olsson, T. S., Hartley, M., Dean, C., & Rosa, S. (2016). A method for detecting single mRNA molecules in arabidopsis thaliana. *Plant Methods, 12*(1), 13.

Dye, M., Buchanan, L., Dorofaeff, F., & Beecroft, F. (1983). Die-back of apricot trees following soil application of boron. *New Zealand Journal of Experimental Agriculture, 11*(4), 331-342.

Fenech, M., Kirsch-Volders, M., Natarajan, A. T., Surralles, J., Crott, J. W., Parry, J., . . . Thomas, P. (2011). Molecular mechanisms of micronucleus, nucleoplasmic bridge and nuclear bud formation in mammalian and human cells. *Mutagenesis, 26*(1), 125-132. doi:10.1093/mutage/geq052 [doi]

Foreman, J., Demidchik, V., Bothwell, J. H., Mylona, P., Miedema, H., Torres, M. A., . . . Jones, J. D. (2003). Reactive oxygen species produced by NADPH oxidase regulate plant cell growth. *Nature, 422*(6930), 442-446.

Fu, H., Reis, N., Lee, Y., Glickman, M. H., & Vierstra, R. D. (2001). Subunit interaction maps for the regulatory particle of the 26S proteasome and the COP9 signalosome. *The EMBO Journal, 20*(24), 7096-7107. doi:10.1093/emboj/20.24.7096 [doi]

Fujiwara, T., Hirai, M. Y., Chino, M., Komeda, Y., & Naito, S. (1992). Effects of sulfur nutrition on expression of the soybean seed storage protein genes in transgenic petunia. *Plant Physiology, 99*(1), 263-268.

Goebl, M., & Yanagida, M. (1991). The TPR snap helix: A novel protein repeat motif from mitosis to transcription. *Trends in Biochemical Sciences, 16*, 173-177.

Goli, E., Hiemstra, T., Van Riemsdijk, W. H., Rahnemaie, R., & Malakouti, M. J. (2010). Diffusion of neutral and ionic species in charged membranes: Boric acid, arsenite, and water. *Analytical Chemistry, 82*(20), 8438-8445.

Grieneisen, V. A., Xu, J., Marée, A. F., Hogeweg, P., & Scheres, B. (2007). Auxin transport is sufficient to generate a maximum and gradient guiding root growth. *Nature, 449*(7165), 1008-1013.

Grieneisen, V. A., Scheres, B., Hogeweg, P., & M Maree, A. F. (2012). Morphogengineering roots: Comparing mechanisms of morphogen gradient formation. *BMC Systems Biology, 6*, 37-0509-6-37. doi:10.1186/1752-0509-6-37 [doi]

Guyomarc'h, S., Vernoux, T., Traas, J., Zhou, D. X., & Delarue, M. (2004). MGOUN3, an arabidopsis gene with TetratricoPeptide-repeat-related motifs, regulates meristem cellular organization. *Journal of Experimental Botany, 55*(397), 673-684. doi:10.1093/jxb/erh069 [doi]

Heath, R. L., & Packer, L. (1968). Steady-state fluorescence of spinach chloroplasts and electron flow. *Archives of Biochemistry and Biophysics, 125*(3), 1019-1022.

Heidstra, R., Welch, D., & Scheres, B. (2004). Mosaic analyses using marked activation and deletion clones dissect arabidopsis SCARECROW action in asymmetric cell division. *Genes & Development, 18*(16), 1964-1969. doi:10.1101/gad.305504 [doi]

Helariutta, Y., Fukaki, H., Wysocka-Diller, J., Nakajima, K., Jung, J., Sena, G., . . . Benfey, P. N. (2000). The< i> SHORT-ROOT</i> gene controls radial patterning of the< i> Arabidopsis</i> root through radial signaling. *Cell, 101*(5), 555-567.

Huffaker, R., & Peterson, L. (1974). Protein turnover in plants and possible means of its regulation. *Annual Review of Plant Physiology, 25*(1), 363-392.

Inagaki, S., Suzuki, T., Ohto, M. A., Urawa, H., Horiuchi, T., Nakamura, K., & Morikami, A. (2006). Arabidopsis TEBICHI, with helicase and DNA polymerase domains, is required for regulated cell division and differentiation in meristems. *The Plant Cell, 18*(4), 879-892. doi:tpc.105.036798 [pii]

Karabal, E., Yücel, M., & Öktem, H. A. (2003). Antioxidant responses of tolerant and sensitive barley cultivars to boron toxicity. *Plant Science, 164*(6), 925-933.

Kasai, K., Takano, J., Miwa, K., Toyoda, A., & Fujiwara, T. (2011). High boron-induced ubiquitination regulates vacuolar sorting of the BOR1 borate transporter in arabidopsis thaliana. *The Journal of Biological Chemistry, 286*(8), 6175-6183. doi:10.1074/jbc.M110.184929 [doi]

Kasajima, I., Ide, Y., Ohkama-Ohtsu, N., Hayashi, H., Yoneyama, T., & Fujiwara, T. (2004). A protocol for rapid DNA extraction fromArabidopsis thaliana for PCR analysis. *Plant Molecular Biology Reporter, 22*(1), 49-52.

Keles, Y., Öncel, I., & Yenice, N. (2004). Relationship between boron content and antioxidant compounds in citrus leaves taken from fields with different water source. *Plant and Soil, 265*(1-2), 345-353.

Koelmel, J., Leland, T., Wang, H., Amarasiriwardena, D., & Xing, B. (2013). Investigation of gold nanoparticles uptake and their tissue level distribution in rice plants by laser ablation-inductively coupled-mass spectrometry. *Environmental Pollution, 174*, 222-228.

Kouchi, H., & Kumazawa, K. (1975). Anatomical responses of root tips to boron deficiency I. effects of boron deficiency on elongation of root tips and their morphological characteristics. *Soil Science and Plant Nutrition, 21*(1), 21-28.

Kramer, E. M., Frazer, N. L., & Baskin, T. I. (2007). Measurement of diffusion within the cell wall in living roots of arabidopsis thaliana. *Journal of Experimental Botany, 58*(11), 3005-3015. doi:erm155 [pii]

Kurepa, J., & Smalle, J. A. (2008). Structure, function and regulation of plant proteasomes. *Biochimie, 90*(2), 324-335.

Kurepa, J., Walker, J. M., Smalle, J., Gosink, M. M., Davis, S. J., Durham, T. L., . . . Vierstra, R. D. (2003). The small ubiquitin-like modifier (SUMO) protein modification system in arabidopsis. accumulation of SUMO1 and -2 conjugates is increased by stress. *The Journal of Biological Chemistry, 278*(9), 6862-6872. doi:10.1074/jbc.M209694200 [doi]

Lam, Y. A., Lawson, T. G., Velayutham, M., Zweier, J. L., & Pickart, C. M. (2002). A proteasomal ATPase subunit recognizes the polyubiquitin degradation signal. *Nature, 416*(6882), 763-767.

Lamb, J. R., Tugendreich, S., & Hieter, P. (1995). Tetratrico peptide repeat interactions: To TPR or not to TPR? *Trends in Biochemical Sciences, 20*(7), 257-259.

Laskowski, M., Grieneisen, V. A., Hofhuis, H., Colette, A., Hogeweg, P., Marée, A. F., & Scheres, B. (2008). Root system architecture from coupling cell shape to auxin transport. *PLoS Biol, 6*(12), e307.

Lefevre, I., VOGEL ‐MIKUŠ, K., Jeromel, L., VAVPETIČ, P., Planchon, S., ARČON, I., . . . Renaut, J. (2014). Differential cadmium and zinc distribution in relation to their physiological impact in the leaves of the accumulating zygophyllum fabago L. *Plant, Cell & Environment, 37*(6), 1299-1320.

Levesque, M. J., & Raj, A. (2013). Single-chromosome transcriptional profiling reveals chromosomal gene expression regulation. *Nature Methods, 10*(3), 246-248.

Marschner, H. (1995). Mineral nutrition of higher plants. 2nd. *Edn.Academic Pres,*

Matoh, T., Ishigaki, K., Mizutani, M., Matsunaga, W., & Takabe, K. (1992). Boron nutrition of cultured tobacco BY-2 cells I. requirement for and intracellular localization of boron and selection of cells that tolerate low levels of boron. *Plant and Cell Physiology, 33*(8), 1135-1141.

Miwa, K., & Fujiwara, T. (2011). Role of overexpressed BOR4, a boron exporter, in tolerance to high level of boron in shoots. *Soil Science and Plant Nutrition, 57*(4), 558-565.

Miwa, K., & Fujiwara, T. (2010). Boron transport in plants: Co-ordinated regulation of transporters. *Annals of Botany, 105*(7), 1103-1108. doi:10.1093/aob/mcq044 [doi]

Miwa, K., Takano, J., Omori, H., Seki, M., Shinozaki, K., & Fujiwara, T. (2007). Plants tolerant of high boron levels. *Science (New York, N.Y.), 318*(5855), 1417. doi:318/5855/1417 [pii]

Miwa, K., Wakuta, S., Takada, S., Ide, K., Takano, J., Naito, S., . . . Fujiwara, T. (2013). Roles of BOR2, a boron exporter, in cross linking of rhamnogalacturonan II and root elongation under boron limitation in arabidopsis. *Plant Physiology, 163*(4), 1699-1709. doi:10.1104/pp.113.225995 [doi]

Miwa, K., Wakuta, S., Takada, S., Ide, K., Takano, J., Naito, S., . . . Fujiwara, T. (2013). Roles of BOR2, a boron exporter, in cross linking of rhamnogalacturonan II and root elongation under boron limitation in arabidopsis. *Plant Physiology, 163*(4), 1699-1709. doi:10.1104/pp.113.225995 [doi]

Molassiotis, A., Sotiropoulos, T., Tanou, G., Diamantidis, G., & Therios, I. (2006). Boron-induced oxidative damage and antioxidant and nucleolytic responses in shoot tips culture of the apple rootstock EM 9 (malus domestica borkh). *Environmental and Experimental Botany, 56*(1), 54-62.

Müller, J., Beck, M., Mettbach, U., Komis, G., Hause, G., Menzel, D., & Šamaj, J. (2010). Arabidopsis MPK6 is involved in cell division plane control during early root development, and localizes to the pre‐prophase band, phragmoplast, trans‐Golgi network and plasma membrane. *The Plant Journal, 61*(2), 234-248.

Müller, S.Plant cell division. *Els,*

Müller, S., Han, S., & Smith, L. G. (2006). Two kinesins are involved in the spatial control of cytokinesis in arabidopsis thaliana. *Current Biology, 16*(9), 888-894.

Nable, R. O., Bañuelos, G. S., & Paull, J. G. (1997). Boron toxicity. *Plant and Soil, 193*(1-2), 181-198.

Noguchi, K., Yasumori, M., Imai, T., Naito, S., Matsunaga, T., Oda, H., . . . Fujiwara, T. (1997). bor1-1, an arabidopsis thaliana mutant that requires a high level of boron. *Plant Physiology, 115*(3), 901-906. doi:115/3/901 [pii]

Ooka, H., Satoh, K., Doi, K., Nagata, T., Otomo, Y., Murakami, K., . . . Kikuchi, S. (2003). Comprehensive analysis of NAC family genes in oryza sativa and arabidopsis thaliana. *DNA Research : An International Journal for Rapid Publication of Reports on Genes and Genomes, 10*(6), 239-247.

Perilli, S., Di Mambro, R., & Sabatini, S. (2012). Growth and development of the root apical meristem. *Current Opinion in Plant Biology, 15*(1), 17-23.

Power, P. P., & Woods, W. G. (1997). The chemistry of boron and its speciation in plants. *Plant and Soil, 193*(1-2), 1-13.

Prasad, B. D., Goel, S., & Krishna, P. (2010). In silico identification of carboxylate clamp type tetratricopeptide repeat proteins in arabidopsis and rice as putative co-chaperones of Hsp90/Hsp70. *PLoS One, 5*(9), e12761.

Punshon, T., Jackson, B. P., Bertsch, P. M., & Burger, J. (2004). Mass loading of nickel and uranium on plant surfaces: Application of laser ablation-ICP-MS. *Journal of Environmental Monitoring, 6*(2), 153-159.

Raj, A., & Tyagi, S. (2010). Detection of individual endogenous RNA transcripts in situ using multiple singly labeled probes. *Methods in Enzymology, 472*, 365-386.

Raven, J. (1980). Short ‐and long ‐distance transport of boric acid in plants. *New Phytologist, 84*(2), 231-249.

Reid, R. J., Hayes, J. E., Post, A., Stangoulis, J. C. R., & Graham, R. D. (2004). A critical analysis of the causes of boron toxicity in plants. *Plant, Cell & Environment, 27*(11), 1405-1414.

Ricaud, L., Proux, C., Renou, J., Pichon, O., Fochesato, S., Ortet, P., & Montané, M. (2007). ATM-mediated transcriptional and developmental responses to γ-rays in arabidopsis. *PloS One, 2*(5), e430.

Rosa, S., Duncan, S., & Dean, C. (2016). Mutually exclusive sense-antisense transcription at FLC facilitates environmentally induced gene repression. *Nature Communications, 7*, 13031. doi:10.1038/ncomms13031 [doi]

Roy, R., Finck, A., Blair, G., & Tandon, H. (2006). Plant nutrition for food security. *A Guide for Integrated Nutrient Management.FAO Fertilizer and Plant Nutrition Bulletin, 16*, 368.

Sagi, M., & Fluhr, R. (2006). Production of reactive oxygen species by plant NADPH oxidases. *Plant Physiology, 141*(2), 336-340. doi:141/2/336 [pii]

Sakamoto, T., Inui, Y. T., Uraguchi, S., Yoshizumi, T., Matsunaga, S., Mastui, M., . . . Fujiwara, T. (2011). Condensin II alleviates DNA damage and is essential for tolerance of boron overload stress in arabidopsis. *The Plant Cell, 23*(9), 3533-3546. doi:10.1105/tpc.111.086314 [doi]

Schindelin, J., Arganda-Carreras, I., Frise, E., Kaynig, V., Longair, M., Pietzsch, T., . . . Schmid, B. (2012). Fiji: An open-source platform for biological-image analysis. *Nature Methods, 9*(7), 676-682.

Shaul, O., Mironov, V., Burssens, S., Van Montagu, M., & Inze, D. (1996). Two arabidopsis cyclin promoters mediate distinctive transcriptional oscillation in synchronized tobacco BY-2 cells. *Proceedings of the National Academy of Sciences of the United States of America, 93*(10), 4868-4872.

Shorrocks, V. M. (1997). The occurrence and correction of boron deficiency. *Plant and Soil, 193*(1-2), 121-148.

Sikorski, R. S., Boguski, M. S., Goebl, M., & Hieter, P. (1990). A repeating amino acid motif in CDC23 defines a family of proteins and a new relationship among genes required for mitosis and RNA synthesis. *Cell, 60*(2), 307-317.

Sinha, P., Dube, B., Singh, M., & Chatterjee, C. (2006). Effect of boron stress on yield, biochemical parameters and quality of tomato. *Indian Journal of Horticulture, 63*(1), 39-43.

Slewinski, T. L. (2011). Diverse functional roles of monosaccharide transporters and their homologs in vascular plants: A physiological perspective. *Molecular Plant, 4*(4), 641-662.

Smalle, J., & Vierstra, R. D. (2004). The ubiquitin 26S proteasome proteolytic pathway. *Annu.Rev.Plant Biol., 55*, 555-590.

Stangoulis, J. C., Reid, R. J., Brown, P. H., & Graham, R. D. (2001). Kinetic analysis of boron transport in chara. *Planta, 213*(1), 142-146.

Sugiyama, Y., Fukui, M., Kikuchi, M., Hasebe, K., Nakayama, A., Nishinari, K., . . . Yukawa, S. (2008). Traffic jams without bottlenecks—experimental evidence for the physical mechanism of the formation of a jam. *New Journal of Physics, 10*(3), 033001.

Suzuki, T., Inagaki, S., Nakajima, S., Akashi, T., Ohto, M., Kobayashi, M., . . . Tabata, S. (2004). A novel arabidopsis gene TONSOKU is required for proper cell arrangement in root and shoot apical meristems. *The Plant Journal, 38*(4), 673-684.

Suzuki, T., Nakajima, S., Inagaki, S., Hirano-Nakakita, M., Matsuoka, K., Demura, T., . . . Nakamura, K. (2005). TONSOKU is expressed in S phase of the cell cycle and its defect delays cell cycle progression in arabidopsis. *Plant & Cell Physiology, 46*(5), 736-742. doi:pci082 [pii]

Takano, J., Noguchi, K., Yasumori, M., Kobayashi, M., Gajdos, Z., Miwa, K., . . . Fujiwara, T. (2002). Arabidopsis boron transporter for xylem loading. *Nature, 420*(6913), 337-340.

Takano, J., Yamagami, M., Noguchi, K., Hayashi, H., & Fujiwara, T. (2001). Preferential translocation of boron to young leaves in arabidopsis thaliana regulated by the BOR1 gene. *Soil Science and Plant Nutrition, 47*(2), 345-357.

Takano, J., Miwa, K., Yuan, L., von Wiren, N., & Fujiwara, T. (2005). Endocytosis and degradation of BOR1, a boron transporter of arabidopsis thaliana, regulated by boron availability. *Proceedings of the National Academy of Sciences of the United States of America, 102*(34), 12276-12281. doi:0502060102 [pii]

Takano, J., Tanaka, M., Toyoda, A., Miwa, K., Kasai, K., Fuji, K., . . . Fujiwara, T. (2010). Polar localization and degradation of arabidopsis boron transporters through distinct trafficking pathways. *Proceedings of the National Academy of Sciences of the United States of America,*

Takano, J., Wada, M., Ludewig, U., Schaaf, G., von Wiren, N., & Fujiwara, T. (2006). The arabidopsis major intrinsic protein NIP5;1 is essential for efficient boron uptake and plant development under boron limitation. *The Plant Cell, 18*(6), 1498-1509. doi:tpc.106.041640 [pii]

Takeda, S., Tadele, Z., Hofmann, I., Probst, A. V., Angelis, K. J., Kaya, H., . . . Paszkowski, J. (2004). BRU1, a novel link between responses to DNA damage and epigenetic gene silencing in arabidopsis. *Genes & Development, 18*(7), 782-793. doi:10.1101/gad.295404 [doi]

Tanaka, M., Sotta, N., Yamazumi, Y., Yamashita, Y., Miwa, K., Murota, K., . . . Fujiwara, T. (2016). The minimum open reading frame, AUG-stop, induces boron-dependent ribosome stalling and mRNA degradation. *The Plant Cell,* doi:tpc.00481.2016 [pii]

Tanaka, M., Takano, J., Chiba, Y., Lombardo, F., Ogasawara, Y., Onouchi, H., . . . Fujiwara, T. (2011). Boron-dependent degradation of NIP5;1 mRNA for acclimation to excess boron conditions in arabidopsis. *The Plant Cell, 23*(9), 3547-3559. doi:10.1105/tpc.111.088351 [doi]

Tanaka, M., Wallace, I. S., Takano, J., Roberts, D. M., & Fujiwara, T. (2008). NIP6;1 is a boric acid channel for preferential transport of boron to growing shoot tissues in arabidopsis. *The Plant Cell, 20*(10), 2860-2875. doi:10.1105/tpc.108.058628 [doi]

Torres, M. A., Onouchi, H., Hamada, S., Machida, C., Hammond‐Kosack, K. E., & Jones, J. D. (1998). Six arabidopsis thaliana homologues of the human respiratory burst oxidase (gp91phox). *The Plant Journal, 14*(3), 365-370.

Traas, J., Bellini, C., Nacry, P., Kronenberger, J., Bouchez, D., & Caboche, M. (1995). Normal differentiation patterns in plants lacking microtubular preprophase bands.

Van den Berg, C., Willemsen, V., Hendriks, G., Weisbeek, P., & Scheres, B. (1997). Short-range control of cell differentiation in the arabidopsis root meristem. *Nature, 390*(6657), 287-289.

Vierstra, R. D. (1993). Protein degradation in plants. *Annual Review of Plant Biology, 44*(1), 385-410.

Vierstra, R. D. (2003). The ubiquitin/26S proteasome pathway, the complex last chapter in the life of many plant proteins. *Trends in Plant Science, 8*(3), 135-142.

Walker, K. L., Müller, S., Moss, D., Ehrhardt, D. W., & Smith, L. G. (2007). Arabidopsis TANGLED identifies the division plane throughout mitosis and cytokinesis. *Current Biology, 17*(21), 1827-1836.

Wang, S., Brown, R., & Gray, D. (1994). Application of laser ablation-ICPMS to the spatially resolved micro-analysis of biological tissue. *Applied Spectroscopy, 48*(11), 1321-1325.

Wolf, D. H., & Hilt, W. (2004). The proteasome: A proteolytic nanomachine of cell regulation and waste disposal. *Biochimica Et Biophysica Acta (BBA)-Molecular Cell Research, 1695*(1), 19-31.

Woods, W. G. (1996). Review of possible boron speciation relating to its essentiality. *The Journal of Trace Elements in Experimental Medicine, 9*(4), 153-163.

Xu, X. M., Zhao, Q., Rodrigo-Peiris, T., Brkljacic, J., He, C. S., Muller, S., & Meier, I. (2008). RanGAP1 is a continuous marker of the arabidopsis cell division plane. *Proceedings of the*

National Academy of Sciences of the United States of America, 105(47), 18637-18642. doi:10.1073/pnas.0806157105 [doi]

Yamaguchi, M., Nagahage, I. S. P., Ohtani, M., Ishikawa, T., Uchimiya, H., Kawai-Yamada, M., & Demura, T. (2015). Arabidopsis NAC domain proteins VND-INTERACTING1 and ANAC103 interact with multiple NAC domain proteins. *Plant Biotechnology,* (0)

Yi, D., Alvim Kamei, C. L., Cools, T., Vanderauwera, S., Takahashi, N., Okushima, Y., . . . De Veylder, L. (2014). The arabidopsis SIAMESE-RELATED cyclin-dependent kinase inhibitors SMR5 and SMR7 regulate the DNA damage checkpoint in response to reactive oxygen species. *The Plant Cell, 26*(1), 296-309. doi:10.1105/tpc.113.118943 [doi]

Yoshiyama, K., Conklin, P. A., Huefner, N. D., & Britt, A. B. (2009). Suppressor of gamma response 1 (SOG1) encodes a putative transcription factor governing multiple responses to DNA damage. *Proceedings of the National Academy of Sciences of the United States of America, 106*(31), 12843-12848. doi:10.1073/pnas.0810304106 [doi]

Yoshiyama, K. O., Kobayashi, J., Ogita, N., Ueda, M., Kimura, S., Maki, H., & Umeda, M. (2013). ATM-mediated phosphorylation of SOG1 is essential for the DNA damage response in arabidopsis. *EMBO Reports, 14*(9), 817-822. doi:10.1038/embor.2013.112 [doi]

Acknowledgement

I have been a research fellow of the Japan Society for the Promotion of Science for two years since April 2015, and researches in this thesis were supported in part by JSPS KAKENHI Grant Number 15J11021. I acknowledge ABRC for distributing T-DNA mutant seeds.

I thank Drs. Shinichiro Sawa, Ryo Tabata, Masashi Yamada, Mitsuyasu Hasebe, Shuji Shigenobu, Katsushi Yamaguchi for whole genome sequencing, and Dr. Masami Y. Hirai for microarray analysis, and Dr. Akie Shimotohno for conducting LA-ICP-MS analysis and Tsuneo Hakoyama for his support, and Dr. Susan Duncan for smFISH analysis. I acknowledge contribution of Mr. Lukram Shantikumar in analyzing *TPR5* gene, and of Mr. Takafumi Sato and Dr. Micol De Ruvo in establishing the mathematical models. I owe a very important debt to Dr. Takuya Sakamoto for his continuous support, including establishment of *rpt5a* suppressor mutants and EdU uptake assay, and Dr. Sachihiro Matsunaga for his advice. I appreciate technical assistance from Mses. Yuko Kawara, Yayoi T. Inui and Jun Itami. I also acknowledge support and helpful comments from Drs. Koji Kasai, Takehiro Kamiya, Yoshihiro Omori and Mayuki Tanaka. I would like to express my gratitude to Drs. Akiko Satake and Motohide Seki for helping my first step of mathematical analysis, which enabled my study later on.

I would like to express my deepest appreciation to Dr. Toru Fujiwara for 6 years of encouraging supervision, providing me with opportunities for various experiences. Special thanks also to Drs. Athanasius F.M. Marée and Verônica A. Grieneisen, for their patient and warm support.

I am deeply grateful to all the members of Fujiwara laboratory in the University of Tokyo, and Computational and Systems Biology department in John Innes Centre.